

INFORMATION TO USERS

This manuscript has been reproduced from the microfilm master. UMI films the text directly from the original or copy submitted. Thus, some thesis and dissertation copies are in typewriter face, while others may be from any type of computer printer.

The quality of this reproduction is dependent upon the quality of the copy submitted. Broken or indistinct print, colored or poor quality illustrations and photographs, print bleedthrough, substandard margins, and improper alignment can adversely affect reproduction.

In the unlikely event that the author did not send UMI a complete manuscript and there are missing pages, these will be noted. Also, if unauthorized copyright material had to be removed, a note will indicate the deletion.

Oversize materials (e.g., maps, drawings, charts) are reproduced by sectioning the original, beginning at the upper left-hand corner and continuing from left to right in equal sections with small overlaps.

Photographs included in the original manuscript have been reproduced xerographically in this copy. Higher quality 6" x 9" black and white photographic prints are available for any photographs or illustrations appearing in this copy for an additional charge. Contact UMI directly to order.

**Bell & Howell Information and Learning
300 North Zeeb Road, Ann Arbor, MI 48106-1346 USA
800-521-0600**

UMI[®]

UNIVERSITY OF OKLAHOMA

GRADUATE COLLEGE

**DIGITAL SIGNAL PROCESSING ON THE UNIT
SPHERE VIA A RAMANUJAN SET OF ROTATIONS
AND PLANAR WAVELETS**

A Dissertation

SUBMITTED TO THE GRADUATE FACULTY

in partial fulfillment of the requirements for the

degree of

Doctor of Philosophy

By

MOHAMED ALLALI

Norman, Oklahoma

2000

UMI Number: 9975791

UMI[®]

UMI Microform 9975791

Copyright 2000 by Bell & Howell Information and Learning Company.

All rights reserved. This microform edition is protected against
unauthorized copying under Title 17, United States Code.

Bell & Howell Information and Learning Company
300 North Zeeb Road
P.O. Box 1346
Ann Arbor, MI 48106-1346

©Copyright By MOHAMED ALLALI 2000

All Rights Reserved

**DIGITAL SIGNAL PROCESSING ON THE UNIT SPHERE
VIA A RAMANUJAN SET OF ROTATIONS AND PLANAR WAVELETS**

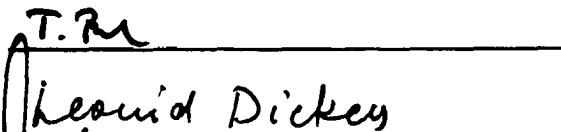
A DISSERTATION

APPROVED FOR THE GRADUATE COLLEGE

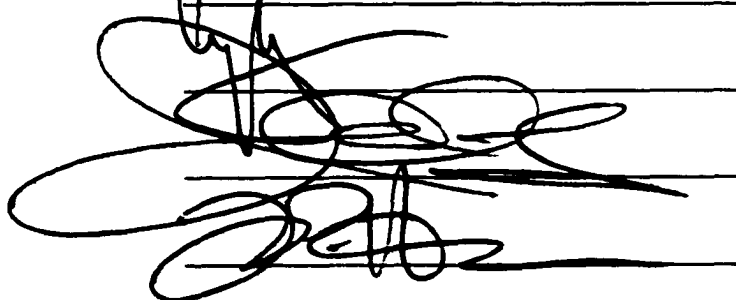
Approved By



T. R.



Leavid Dickey



ACKNOWLEDGEMENTS

Praise be to Allah, Lord of the worlds who made this work possible. I praise Him for His favors and ask Him to increase His grace and generosity.

I would like to thank my two advisors Professors Victor DeBrunner and Tomasz Przebinda for their advice, guidance, and assistance throughout this work. Indeed, words are inadequate to express my deep gratitude and appreciation to them for being a constant source of encouragement and patience throughout my graduate studies.

Additionally, many thanks are due to Professor Joseph Havlicek for a very careful revision of this work. I thank Professors Leonid Dickey, John Cheung, and Gerard Walschap for their willingness to serve on my committee.

Many people whom I talked to gave very useful pointers and provided additional encouragement. For this I am indebted to Professors Murad Özaydin, Paul Goodey and Leonard Rubin.

Very special thanks go to my dear friend Mostafa El Hamly from the Meteorology Department. His kindness and help during my stay in Norman have made the years here even more memorable.

I could not have completed this dissertation without the support, encouragement and understanding of my wife Farah Sabri.

Finally, I wish to dedicate this dissertation to my father Houssine, to my mother Fatima, to my brothers Youssef and Tarik and to my sister Imane. Without their love, support, encouragement and prayers throughout the years, I would never have made it this far.

TABLE OF CONTENTS

Chapter 1: Introduction	1
Chapter 2: Interpolation on the unit sphere	8
2.1 Positive definite functions	8
2.2 Strictly positive definite functions	11
2.3 Examples of strictly positive definite functions	18
2.4 The interpolation problem	19
Chapter 3: A Ramanujan set of rotations	20
Chapter 4: Equidistribution on the unit sphere	25
4.1 Equidistribution via a Ramanujan set of rotations	25
4.2 Numerical results	28
Chapter 5: Covering the unit sphere	31
Chapter 6: One dimensional wavelets	42
6.1 Wavelets on the real line	43
6.2 Two wavelet-based indices for abrupt changes detection	50
Chapter 7: Two dimensional wavelets	58
Chapter 8: Compression on the unit sphere	61
8.1 Image compression	61
8.2 Pseudocode for compression	63
8.3 An example of data compression on the unit sphere	65
8.4 A general method for spherical compression	72
Chapter 9: Concluding remarks	83

References	85
Appendix A: Code for generating points on the unit sphere	89
Appendix B: Code for frequency-hopped signals	91
Appendix C: Code for chirp signals	97

Chapter 1

Introduction

The past four decades have witnessed a phenomenally rapid development of methods in digital signal processing in mathematical, statistical, biomedical, and engineering communities. Wavelets, for example, in the Euclidean space have been proven particularly powerful for compressing images [D-J-L], for detecting transient patterns and singularities [M-H], for estimating signals of complex structures from noisy measurements [Do], and for multiscale dynamic modeling and forecasting of time series [L-H].

Similar applications, including data compression, singularity detection, interpolation, function estimation, also demand methods for handling spherical data that occur in computer graphics, climatology and environmental sciences.

The direction that we took in our doctoral work was to contribute to research in the field of digital signal processing on the sphere. Our studies center on interpolation, equidistribution, covering and compression on the sphere.

Because this dissertation is an interdisciplinary work in Mathematics and Electrical and Computer Engineering, it represents a synthesis of ideas from the described fields of science and engineering.

First, we study the problem of interpolating data on the sphere. Data interpolation problems, where the underlying domain is the sphere, arise in many areas such as geophysics where the unit sphere is taken as a model of the earth. In recent years there has been a great deal of interest in radial basis functions (RBF's) as a tool for interpolation. Normally, a radial basis function is the composition of a univariate function with some sort of a distance function. That is to say, an RBF is a function of only the distance between points on the unit sphere. The interest in RBF's was inspired by the observation [Fr] that in the bivariate setting, they are among the most effective methods for interpolation and approximation of scattered data. Their use was also encouraged by the fact that radial basis methods are extremely easy to program in any number of variables [D-Mi].

The problem of interpolation on the sphere is stated in Chapter 2 of this thesis where it is shown that it is related to the notion of strictly positive definite functions. We give first definitions of positive definite functions in the case of the real line and in the case of the m -sphere. Then after defining strictly positive definite functions, we give a sufficient condition for a zonal function to be a strictly positive definite.

In 1992, Xu and Cheney [X-C] showed that if all of the Legendre coefficients of a zonal function on a sphere are positive, then the strict positive

definiteness is guaranteed. However, in 1997, Schreiner [S] proved the same result with the weakened hypothesis that finitely many Legendre coefficients can be zero. A major result of this thesis is that we have proven the same result as a consequence of a more general representation-theoretic result, namely for compact groups using tools from the Representation Theory.

The other major direction of this thesis is to compress square integrable functions on the unit sphere. The main tools used in this analysis are a Ramanujan set of rotations and planar wavelets. Ramanujan sets of rotations are introduced in Chapter 3 and our focus is on S_5^M , a special set from the Ramanujan set of rotations. Starting with a point on the digital sphere lying on none of the coordinate axes and using S_5^M we can generate points on the sphere. The equidistribution of these generated points is studied in Chapters 4 and 5.

We show the uniformity of this distribution in terms of quadrature on the sphere. Furthermore, the method of expanding a function into a Fourier series in terms of specific functions such as spherical harmonics or radial basis functions amounts to the problem of evaluating the expansion coefficients by integration. Hence, an approximate integration can be simply performed by the computation of the mean of the functional values at those points generated by S_5^M .

In the algorithm proposed in Chapter 8, the method of covering the sphere by means of spherical caps of fixed radius is needed. Therefore we derive in Chapter 5 a precise formula to cover the unit sphere with a given radius. To find the optimal number (the minimal number of spherical caps) required is still an open problem.

In Chapters 6 and 7 one dimensional and two dimensional wavelets are introduced. Wavelets, simply put, are scaled and translated copies of a particular window function called the mother wavelet. They have proven to be a powerful and flexible tool for computations and data reduction. Their power lies in the fact that they only require a small number of coefficients to represent general functions and large data sets accurately. This allows for compression and efficient computations [D-J-L], [C-M-Q-W]. Classically, wavelet constructions have been employed on infinite domains (such as the real line \mathbb{R} or the plane \mathbb{R}^2). Since most practical computations are confined to finite domains, a number of boundary constructions have also been developed.

The representation of a signal by means of its spectrum or Fourier transform is essential in solving many problems both in pure mathematics and in applied science. However, it is in some instances not the most natural or useful way of representing a signal. The Fourier transform contains informa-

tion about the frequencies of the entire signal, but does not show how they vary with time. In contrast, wavelet analysis provides a simple and effective approach for dealing with the local aspects of a signal.

In particular, we will study in Chapter 6 a common problem in signal processing which is the ability to detect abrupt changes in very short segments that are not strictly stationary. A method based on time-frequency representations (TFRs) for detecting abrupt spectral changes in noisy signals was recently introduced [L-D]. The paper presents a stationarity index derived from the spectrogram of the signal.

Our proposed method in this dissertation is an improvement to this previous method by deriving the stationarity index from the spectrogram of the wavelet coefficients of the signal or from the coefficients themselves rather than from the spectrogram of the signal. We have considered this modification due to the fact that the wavelet transform is a useful tool for non-stationary signal analysis that has found many applications in time-frequency analysis [F1] and transient detection [M-H]. After defining the new modified stationarity indices, we consider two kinds of signals from [L-D], namely test signals presenting very short frequency-hopped segments and chirp signals corrupted with noise. Comparisons between the original method and the new method are performed for different levels of noise.

The problem of constructing a wavelet-like theory for the sphere in a Euclidean space, has attracted a lot of interest in the last five years [S-S], [F-W]. However, wavelet type constructions for more general manifolds have only recently been attempted and are still in their infancy. Although from a topological point of view the sphere, $S^2 \subseteq \mathbb{R}^3$, appears to be a simple manifold, wavelet techniques from \mathbb{R}^2 do not easily extend to the unit sphere as there is no single chart mapping it diffeomorphically onto some open domain in \mathbb{R}^2 .

A number of works extend to S^2 the discrete wavelet scheme based on a multiresolution analysis, using adapted interpolation methods and splines functions [D-D-S-W]. This approach is in general motivated by numerical considerations, but often leads to difficulties around the poles. Others [P-S-T], [F-W] exploit the geometry of the sphere, as encoded in the system of spherical harmonics, but as a result their analyzing functions are poorly localized. However, since the construction of wavelets on general open domains in \mathbb{R}^n or on manifolds is still an open problem, many numerical applications have to assume simple and often unrealistic geometries. Major difficulties arise from the fact that no more Fourier transform techniques are available unless the underlying domain is the entire plane \mathbb{R}^n or the torus $\mathbb{R}^n/\mathbb{Z}^n$.

We do not construct in this thesis a wavelet-like theory for the sphere

such as the multiresolution analysis discussed in Chapters 6 and 7. Rather, we construct an algorithm using planar wavelets and the Ramanujan set of rotations S_5^M to compress functions on the unit sphere. The details about the algorithm are to be found in Chapter 8.

Chapter 2

Interpolation on the Unit Sphere

We are motivated by the problem of interpolating scattered data on the unit sphere using radial basis functions (RBFs) that are only functions of the distance between points on the unit sphere. The interpolation problem can be solved if we introduce the notion of strictly definite positive functions.

In this chapter we define strictly positive definite functions and give sufficient conditions for their existence. Furthermore, we relate them to the interpolation problem.

2.1 Positive definite functions

First, we recall the definition of the one-dimensional Fourier transform.

Definition 2.1.1. *Let f be a real or complex function of one real variable with $f \in L^1(\mathbf{R})$, which means that the Lebesgue integral $\int_{-\infty}^{\infty} |f(x)| dx$ exists and is finite. The Fourier transform of f , denoted by \hat{f} , is a function defined by*

$$\hat{f}(\xi) = \frac{1}{\sqrt{2\pi}} \int_{-\infty}^{\infty} f(x) e^{-ix\xi} dx,$$

where i stands for the imaginary unit.

Here we only mention the fact that if also $\hat{f} \in L^1(\mathbf{R})$, then f can be

recovered from \hat{f} by means of the following inversion formula:

$$f(x) = \frac{1}{\sqrt{2\pi}} \int_{-\infty}^{\infty} \hat{f}(\xi) e^{ix\xi} d\xi.$$

The proof is usually done by a limit argument; see [R] for one.

Definition 2.1.2. A function $f : \mathbf{R} \rightarrow \mathbf{R}$ is called *positive definite* if we have, for any numbers $x_1, \dots, x_n \in \mathbf{R}$, and $\tau_1, \dots, \tau_n \in \mathbf{R}$,

$$\sum_{j,k=1}^n \tau_j \tau_k f(x_j - x_k) \geq 0.$$

Let us note that this concept can be related to the perhaps better known notion of positive definite matrices. Namely, for $x_1, \dots, x_n \in \mathbf{R}$, define the $n \times n$ matrix $A = A(f; x_1, x_2, \dots, x_n)$ by setting $a_{jk} = f(x_j - x_k)$. Then f being positive definite means that A is a positive semidefinite matrix for any choice of x_1, \dots, x_n ; that is, $\tau^T A \tau \geq 0$ for any real column vector $\tau \in \mathbf{R}^n$. (In analogy with the terminology for matrices, it would perhaps be more appropriate to say “a positive semidefinite function” instead of “positive definite function,” but we stick to the traditional terminology.)

Nontrivial examples of positive definite functions are not obvious. The following lemma gives a method for producing some using the Fourier transform.

Lemma 2.1.3 [Sa]. Suppose that a real function $\varphi = \hat{\psi}$ is the Fourier

transform of a nonnegative real function $\psi \in L^1(\mathbf{R})$. Then φ is positive definite.

Proof. Let $x_1, \dots, x_n \in \mathbf{R}$, and $\tau_1, \dots, \tau_n \in \mathbf{R}$ be given. We calculate

$$\begin{aligned} \sum_{j,k=1}^n \tau_j \tau_k \varphi(x_j - x_k) &= \frac{1}{\sqrt{2\pi}} \int_{-\infty}^{\infty} \psi(\xi) \sum_{j,k} \tau_j \tau_k e^{-i(x_j - x_k)\xi} d\xi \\ &= \frac{1}{\sqrt{2\pi}} \int_{-\infty}^{\infty} \psi(\xi) \left(\sum_j \tau_j e^{-ix_j \xi} \right) \left(\sum_j \tau_j e^{ix_j \xi} \right) d\xi. \end{aligned}$$

Since all the x_j and τ_j are real, the sum in the second pair of parentheses is the complex conjugate of the one in the first pair of parentheses, and we obtain

$$\sum_{j,k=1}^n \tau_j \tau_k \varphi(x_j - x_k) = \frac{1}{\sqrt{2\pi}} \int_{-\infty}^{\infty} \psi(\xi) \left| \sum_j \tau_j e^{ix_j \xi} \right|^2 d\xi \geq 0.$$

Hence, the lemma is proven. \square

Example 2.1.4. The function $h(x) = e^{-x^2}$ is positive definite as it is the Fourier transform of the function $e^{-\frac{\xi^2}{4}}$.

Let us generalize this notion to S^m . We denote by S^m the unit sphere in the Euclidean space \mathbf{R}^{m+1} . The usual geodesic distance on S^m is denoted by d_m . Thus

$$d_m(x, y) = \arccos(x \cdot y)$$

where $(x \cdot y)$ is the usual dot product in \mathbf{R}^{m+1} .

A continuous function $g : [0, \pi] \rightarrow \mathbf{R}$ is said to be *positive definite* on S^m if, for any $n \in \mathbf{N}$ and for any set of n points x_1, x_2, \dots, x_n in S^m , the $n \times n$ matrix A having elements $A_{ij} = g(d_m(x_i, x_j))$ is nonnegative definite:

$$c^T A c = \sum_{i=1}^n \sum_{j=1}^n c_i c_j g(d_m(x_i, x_j)) \geq 0, \quad c = (c_1, \dots, c_n) \in \mathbf{R}^n.$$

Schoenberg [Sc] has shown that if the function g admits the uniformly convergent series expansion

$$g(t) = \sum_{n=0}^{\infty} k_n P_n(\cos t), \quad t \in [0, \pi],$$

in terms of certain Legendre (or Gegenbauer or ultraspherical) polynomials, a sufficient condition for the positive definiteness of g is that $k_n \geq 0$, $n = 0, 1, \dots$

2.2 Strictly positive definite functions

If the matrices A in the previous definition are positive definite for all n and for all sets of n distinct points x_1, x_2, \dots, x_n in S^m , we say that g is *strictly positive definite* on S^m .

In 1992, Xu and Cheney [X-C] showed that if all of the Legendre coefficients of a zonal function on a sphere are positive, then the function is strictly positive definite. In 1997, Schreiner [S] proved the same result with the weakened hypothesis that finitely many Legendre coefficients can be zero, but there is a problem in the proof of lemma 4.1 [S], see [F-S].

We have proven the same result as a consequence of a more general representation-theoretic result [A-P].

Let G be a compact group, and let $H \subseteq G$ be a closed subgroup, such that the quotient G/H is infinite. Let $f : G \rightarrow \mathbb{C}$ be a continuous function, invariant under the left and right translations by elements of H . We denote the space of all such functions by $C(H \backslash G/H)$.

Definition 2.2.1. *A function f is strictly positive definite if and only if*

$$\sum_{i,j=1}^n c_i \bar{c}_j f(x_i^{-1} x_j) > 0 \quad (2.2.1)$$

for any finite set $\{x_1, x_2, \dots, x_n\} \subseteq G$ such that the cosets $x_1 H, x_2 H, \dots, x_n H \subseteq G/H$ are distinct, and any complex numbers c_1, c_2, \dots, c_n , not all equal to zero.

Let \hat{G} denote the unitary dual of G , [K, 7.3]. This is the set of equivalence classes of irreducible unitary representations of G . For convenience, we choose an irreducible representation for each such class, and identify \hat{G} with the set of these representations. Recall the Fourier transform

$$\hat{f}(\pi) = \pi(f) = \int_G \pi(x) f(x) dx \quad (\pi \in \hat{G}), \quad (2.2.2)$$

where f is any absolutely integrable function on G with respect to the Haar measure dx . Thus each $\pi(f)$ is a linear map on the finite dimensional Hilbert

space \mathcal{H}_π , where the representation π is realized. Let $\mathcal{H}_\pi^H = \{v \in \mathcal{H}_\pi : \pi(h)v = v, h \in H\}$ be the subspace of H -fixed vectors. Let $(G/H)^\wedge = \{\pi \in \hat{G}; \mathcal{H}_\pi^H \neq 0\}$. By the Frobenius reciprocity theorem, $(G/H)^\wedge$ is the subset of \hat{G} , consisting of representations which occur in $L^2(G/H)$, see [K, 8.4].

Proposition 2.2.2. *A function $f \in C(H \backslash G/H)$ is strictly positive definite if $\pi(f) \geq 0$ for all $\pi \in (G/H)^\wedge$, and $\pi(f)|_{\mathcal{H}_\pi^H} > 0$ for all but finitely many $\pi \in (G/H)^\wedge$.*

Here “ $\pi(f) \geq 0$ ” means that the operator $\pi(f)$ is positive semi-definite, i.e. $(\pi(f)v, v) \geq 0$, for any $v \in \mathcal{H}_\pi$, and the statement “ $\pi(f)|_{\mathcal{H}_\pi^H} > 0$ ” means that the restriction of the operator $\pi(f)$ to \mathcal{H}_π^H is positive definite, i.e. $(\pi(f)v, v) > 0$, for any $v \in \mathcal{H}_\pi^H \setminus \{0\}$.

Proof. With the notation (2.2.1), let μ be a bounded measure on G defined by

$$\int_G \phi(x) d\mu(x) = \sum_{i=1}^n c_i \int_H \phi(x_i h) dh,$$

where ϕ is a continuous function on G , and dh is the Haar measure on H , normalized so that the total measure of H is 1. Notice that the support of μ is contained in $\bigcup_{i=1}^n x_i H$, which (by our assumption) is a proper subset of G .

The Fourier transform of μ is defined as in (2.2.2):

$$\pi(\mu) = \int_G \pi(x) d\mu(x) \quad (\pi \in \hat{G}).$$

Recall the Fourier inversion formula, [K, 12.2] or [H-R, 27.40]:

$$\phi(x) = \sum_{\pi \in \hat{G}} d(\pi) \text{tr}(\pi(\phi) \pi(x)^*) \quad (\phi \in C(G), x \in G),$$

where $d(\pi) = \dim \mathcal{H}_\pi$. If each operator $\pi(\phi)$ is positive semi-definite ($\pi(\phi) \geq 0$) then the above Fourier series is absolutely, and hence uniformly, convergent to the continuous function ϕ , (see [H-R, 34.9]). Hence,

$$\begin{aligned} f(x_i^{-1} x_j) &= \sum_{\pi \in \hat{G}} d(\pi) \text{tr}(\pi(f) \pi(x_i^{-1} x_j)^*) \\ &= \sum_{\pi \in \hat{G}} d(\pi) \text{tr}(\pi(x_i) \pi(f) \pi(x_j)^*). \end{aligned}$$

Notice that $\pi(h) \pi(f) = \pi(f) = \pi(f) \pi(h)$ for all $h \in H$. Hence $\pi(f) = P_{\mathcal{H}_\pi^H} \pi(f) = \pi(f) P_{\mathcal{H}_\pi^H}$, where $P_{\mathcal{H}_\pi^H} = \int_H \pi(h) dh$ is the orthogonal projection on \mathcal{H}_π^H . Therefore,

$$f(x_i^{-1} x_j) = \sum_{\pi \in (G/H)^\wedge} d(\pi) \text{tr}(\pi(x_i) P_{\mathcal{H}_\pi^H} \pi(f) (\pi(x_j) P_{\mathcal{H}_\pi^H})^*). \quad (2.2.3)$$

After multiplying both sides of (2.2.3) by $c_i \bar{c}_j$ and summing over the indices i, j , we see that

$$\sum_{i,j=1}^n c_i \bar{c}_j f(x_i^{-1} x_j) = \sum_{\pi \in (G/H)^\wedge} d(\pi) \text{tr}(\pi(\mu) P_{\mathcal{H}_\pi^H} \pi(f) (\pi(\mu) P_{\mathcal{H}_\pi^H})^*).$$

Since $\pi(\mu) = \pi(\mu)P_{\mathcal{H}_\pi}$, the proposition shall follow as soon as we check that

$$\pi(\mu) \neq 0 \text{ for infinitely many } \pi \in (G/H)^\wedge. \quad (2.2.4)$$

Suppose $\mu(\pi) = 0$ for all but finitely many $\pi \in (G/H)^\wedge$. Then, by Fourier inversion, [H-R, 27.40], μ coincides with a finite linear combination of matrix coefficients of irreducible unitary representations of G . Therefore, the space of all left translates of μ is finite dimensional. Hence, there are finitely many elements $y_1, y_2, \dots, y_m \in G$, such that $\cup_{j=1}^m \text{supp } \mu = G$, where $\text{supp } \mu$ stands for the support of μ . Thus $G = \cup_{j=1}^m \cup_{i=1}^n y_j x_i H$, contrary to our assumption that the set G/H is infinite. \square

Suppose that (G, H) is a Gelfand pair, [D, 22.6.2]. Then for each $\pi \in \hat{G}$ and each $f \in C(H \backslash G/H)$, the operator $\pi(f)$ is a constant multiple of the projection $P_{\mathcal{H}_\pi}$: $\pi(f) = \lambda_\pi(f)P_{\mathcal{H}_\pi}$.

Corollary 2.2.3. *If (G, H) is a Gelfand pair, then a function $f \in C(H \backslash G/H)$ is strictly positive definite if $\lambda_\pi(f) > 0$ for all but finitely many $\pi \in (G/H)^\wedge$.*

As is well known, [D, 20.11.4, 22.6.3], $(SO(n), SO(n-1))$ is a Gelfand pair, and the quotient space $SO(n)/SO(n-1)$ coincides with the unit sphere in \mathbb{R}^n . Furthermore, in this case, the scalars $\lambda_\pi(f)$ can be expressed in terms of Legendre polynomials. We explain this in some detail.

Consider the Euclidean space \mathbb{R}^n equipped with the usual dot product. Let

$e_n = (0, 0, \dots, 0, 1) \in \mathbb{R}^n$ be the “north pole” of the unit sphere $S^{n-1} \subseteq \mathbb{R}^n$. Let $G = SO(n)$ be the group of isometries of the dot product, and let $H \subseteq G$ be the stabilizer of e_n . The restriction to the first $n - 1$ coordinates identifies H with $SO(n - 1)$.

It is customary in representation theory to normalize the Haar measure on any compact group to have the total mass 1. Then the total mass of our homogeneous space G/H is also 1. On the other hand the dot product in \mathbb{R}^n forces a normalization of the rotation invariant measure ω on the sphere S^{n-1} so that the area of the sphere $|S^{n-1}| = \int_{S^{n-1}} d\omega \neq 1$. Hence,

$$\int_{S^{n-1}} \phi(\sigma) d\omega(\sigma) = |S^{n-1}| \int_G \phi(ge_n) dg \quad (\phi \in C(S^{n-1})).$$

Therefore the map

$$L^2(G/H) \ni v \rightarrow \phi \in L^2(S^{n-1}), \quad \phi(ge_n) = |S^{n-1}|^{1/2} v(g) \quad (g \in G)$$

is an isometry. This isometry is surjective and commutes with the action of the group G on both spaces. As is well known, [Mü], the space $L^2(S^{n-1})$ decomposes into a direct sum of irreducible subspaces:

$$L^2(S^{n-1}) = \sum_{m=0}^{\infty} L^2(S^{n-1})_m,$$

where $L^2(S^{n-1})_m$ stands for the space of spherical harmonics of degree m .

Let π_m denote the representation of G on the space $\mathcal{H}_{\pi_m} = L^2(S^{n-1})_m$.

Then the subspace $\mathcal{H}_{\pi_m}^H$ is one dimensional, and is spanned by the Legendre function:

$$L_m(\sigma) = P_m(e_n \cdot \sigma) \quad (\sigma \in S^{n-1}),$$

where P_m is the Legendre polynomial of degree m , (see [Mü, Lemma 2, page 16]). Notice that a function $f \in C(H \backslash G/H)$ is uniquely determined by a continuous function F on the interval $[-1, 1]$ by the formula

$$f(g) = F(e_n \cdot ge_n) \quad (g \in G).$$

Notice that $f(g) = F(e_n \cdot ge_n) = F(g^{-1}e_n \cdot e_n) = F(e_n \cdot g^{-1}e_n) = f(g^{-1})$.

In these terms, the constants which occur in the Corollary 2.2.3 can be calculated as follows (see [Mü, Lemma 1 on page 15, and formula (§4.6) on page 29]):

$$\begin{aligned} \lambda_{\pi_m}(f) &= \lambda_{\pi_m}(f)L_m(e_n) = \pi_m(f)L_m(e_n) \\ &= \int_G f(g)L_m(g^{-1}e_n) dg = \int_G F(e_n \cdot ge_n)P_m(e_n \cdot g^{-1}e_n) dg \\ &= \int_G F(e_n \cdot ge_n)P_m(e_n \cdot ge_n) dg = \frac{|S^{n-2}|}{|S^{n-1}|} \int_{-1}^1 F(t)P_m(t)(1-t^2)^{(n-3)/2} dt. \end{aligned}$$

Thus, by the Corollary 2.2.3, the integral kernel operator on $L^2(S^{n-1})$ corresponding to the integral kernel $F(\eta, \sigma) = F(\eta \cdot \sigma)$, $(\eta, \sigma \in S^{n-1})$, is strictly positive definite if $\lambda_{\pi_m} \geq 0$ for all $m \geq 0$, and the inequality is strict for all but finitely many m . Hence, the result of Schreiner [S] is generalized.

We will now list a number of examples of strictly positive definite functions which have been studied by many authors.

2.3 Examples of strictly positive definite functions

Example 2.3.1. Radial basis functions (RBFs)

- 1 . Gaussians, Hardy multiquadratic, inverse Hardy multiquadratic, and completely monotonic functions of r^2 (Micchelli [Mi]).
- 2 . Compactly supported RBFs (Narcowich and Ward [N-W], Wendland [We], Schaback and Wu [S-W], and Wu [Wu]).

Example 2.3.2. Periodic basis functions (PBFs)

- 1 . Periodic functions having positive Fourier coefficients.

Example 2.3.3. Spherical basis functions (SBFs)

- 1 . $\exp(\cos(\theta))$. Here and below $\theta = \theta(p, q)$ is the geodesic distance on the m -sphere between points p and q .

- 2 . $\sum_{l=0}^{\infty} \sum_{m=1}^{d_l} a_{l,m} Y_{l,m}(p) \overline{Y_{l,m}(q)}$, where the $Y_{l,m}$'s are spherical harmonics on S^m , $a_{l,m} > 0$, and d_l is the dimension of the space of spherical harmonics of order l .

- 3 . $\sum_{l=0}^{\infty} a_l P_l(m+1, \cos(\theta))$, $a_l > 0$ (Xu and Cheney [X-C]).

Example 2.3.4. Strictly positive definite functions on $SO(3)$

- 1 . $e^{\gamma \cos^2 \theta} F(\varphi, \psi, \theta)$, $\gamma > 0$ (Gutzmer [Gu]). φ, θ, ψ are Euler angles, and $F(\varphi, \psi, \theta) := \cos \varphi \cos \psi - (1 - \sin \varphi \sin \psi) \cos \theta - \sin \theta (\sin \varphi + \sin \psi)$.

2.4 Interpolation problem

We will see now how the notion of strictly positive definite functions is related to the interpolation problem.

Assume that a function $F : S^m \rightarrow \mathbb{R}$ is known at finitely many distinct points $\eta_1, \dots, \eta_n \in S^m$ and one looks for an interpolant F_{int} of the form

$$F_{int}(\xi) = \sum_{j=1}^N c_j g(d_m(\xi, \eta_j)), \quad \xi \in S^m$$

satisfying the interpolation conditions $F_{int}(\eta_i) = F(\eta_i)$, $i = 1, \dots, N$. Then the linear system to be solved is

$$\begin{pmatrix} g(d_m(\eta_1, \eta_1)) & \dots & g(d_m(\eta_N, \eta_1)) \\ \vdots & \ddots & \vdots \\ g(d_m(\eta_1, \eta_N)) & \dots & g(d_m(\eta_N, \eta_N)) \end{pmatrix} \begin{pmatrix} c_1 \\ \vdots \\ c_N \end{pmatrix} = \begin{pmatrix} F(\eta_1) \\ \vdots \\ F(\eta_N) \end{pmatrix}.$$

If g is strictly positive definite then the matrix is positive definite, i.e. the interpolation problem is solvable. The numerical inversion is stable and can be effected by a variety of well-understood methods, including iterative procedures and the Cholesky factorization.

The problem of completely characterizing functions which are strictly positive definite on the sphere remains open [F-S].

Chapter 3

A Ramanujan Set of Rotations

In order to study covering, equidistribution and compression on the unit sphere, we shall introduce a special set called the Ramanujan set of rotations due to Lubotzky et al. [L-P-S].

Consider the three dimensional Euclidean vector space \mathbb{R}^3 with the usual dot product, and the corresponding norm of a vector:

$$x \cdot y = x_1y_1 + x_2y_2 + x_3y_3, \quad |x| = \sqrt{x \cdot x},$$
$$(x = (x_1, x_2, x_3), y = (y_1, y_2, y_3) \in \mathbb{R}^3).$$

Let $S^2 = \{x \in \mathbb{R}^3; |x| = 1\}$ be the unit sphere and let $d\sigma$ denote the usual rotation invariant measure on S^2 defined by

$$\int_{\mathbb{R}^3} f(x) dx = \int_0^\infty \int_{S^2} f(r\sigma) d\sigma r^2 dr,$$

where f is a continuous compactly supported function on \mathbb{R}^3 .

We are interested in the Hilbert space $L^2(S^2)$ of square integrable functions on the sphere, with the usual scalar product:

$$(f, g) = \int_{S^2} f(\sigma)\overline{g(\sigma)} d\sigma \quad (f, g \in L^2(S^2)).$$

The corresponding norm of a function $f \in L^2(S^2)$ is $\|f\| = \sqrt{(f, f)}$. The group $G = SO(3)$ of proper rotations preserving the dot product, acts on

this space as follows:

$$\rho(\gamma)f(\sigma) = f(\gamma^{-1}\sigma) \quad (\gamma \in G, \sigma \in S^2, f \in L^2(S^2)). \quad (3.1)$$

Each operator $\rho(\gamma)$ defined in (3.1) is unitary. For any $f, g \in L^2(S^2)$ the function $G \ni \gamma \rightarrow (\rho(\gamma)f, g) \in \mathbb{C}$ is continuous. Moreover, $\rho(\gamma_1)\rho(\gamma_2) = \rho(\gamma_1\gamma_2)$ for any $\gamma_1, \gamma_2 \in G$. In other words, $(\rho, L^2(S^2))$ is a unitary representation of the group G , see [K]. As such, it decomposes into a Hilbert direct sum of irreducible representations. Since this decomposition resembles the decomposition $L^2(\mathbb{R}) = \sum_{j \in \mathbb{Z}} W_j$, we shall describe it briefly.

Let $\mathcal{P} = \mathcal{P}(\mathbb{R}^3)$ denote the space of complex valued polynomial functions on \mathbb{R}^3 . A polynomial $f \in \mathcal{P}$ is called homogeneous of degree n if $f(rx) = r^n f(x)$ for all $r \in \mathbb{R}$ and all $x \in \mathbb{R}^3$. Let $\Delta = \frac{\partial^2}{\partial x_1^2} + \frac{\partial^2}{\partial x_2^2} + \frac{\partial^2}{\partial x_3^2}$ denote the Laplacian. A polynomial $f \in \mathcal{P}$ is called harmonic if $\Delta f = 0$. Let $\mathcal{HP}_n \subseteq \mathcal{P}$ denote the subspace of harmonic polynomials which are homogeneous of degree $n = 0, 1, 2, \dots$. Let \mathcal{H}_n denote the space of functions on S^2 obtained by restricting the elements of \mathcal{HP}_n to S^2 . The theory of spherical harmonics asserts that $L^2(S^2)$ is a Hilbert direct sum of the finite dimensional subspaces \mathcal{H}_n :

$$L^2(S^2) = \sum_{n=0}^{\infty} \mathcal{H}_n,$$

and that the restriction ρ_n of the representation ρ to \mathcal{H}_n is irreducible, for

each $n = 0, 1, 2, \dots$. Moreover, $\dim \mathcal{H}_n = 2n + 1$. For more details and proofs see [Mü].

Let $S \subseteq SO(3)$ be a finite symmetric set. In other words, the number of elements of S , denoted by $|S| = 2N$, is even and $\gamma \in S$ if and only if $\gamma^{-1} \in S$. Let $(T_S f)(x) = \sum_{\gamma \in S} f(\gamma x)$, where $f \in L^2(S^2)$. We would like to approximate the projection $P_{\mathcal{H}_0}$ by $\frac{1}{|S|} T_S$ for suitable S . The first problem is to agree on a way to measure the error for such an approximation. For an operator $T : L^2(S^2) \rightarrow L^2(S^2)$ let $\| T \|$ be the operator norm of T . Explicitly, $\| T \|$ is the supremum of the numbers $\| T(f) \|$, where $f \in L^2(S^2)$ and $\| f \| = (\int |f(x)|^2 dx)^{\frac{1}{2}} = 1$. We agree that our approximation is best when the norm

$$\left\| \frac{1}{|S|} T_S - P_{\mathcal{H}_0} \right\|$$

is minimal. Furthermore, let $u(x) = 1$, $x \in S^2$, denote the unit function.

Thus $\mathcal{H}_0 = \mathbf{C}u$. The orthogonal projection $P_{\mathcal{H}_0} : L^2(S^2) \rightarrow \mathcal{H}_0$ is given by:

$$P_{\mathcal{H}_0} f = \left(\frac{1}{4\pi} \int_{S^2} f(x) dx \right) u \quad (f \in L^2(S^2)).$$

Theorem 3.1 [L-P-S]. *For any finite symmetric set $S \subseteq SO(3)$*

$$\left\| \frac{1}{|S|} T_S - P_{\mathcal{H}_0} \right\| \geq 2 \frac{\sqrt{|S| - 1}}{|S|}.$$

A set where the equality holds is called a **Ramanujan set**. Let p be a prime, equal to 1 modulo 4. Then there exists in [L-P-S] an explicitly described Ramanujan set, S_p , with $|S_p| = p + 1$.

Let S_p be a Ramanujan set, $S_p = \{\gamma_1, \dots, \gamma_{\frac{p+1}{4}}, \gamma_1^{-1}, \dots, \gamma_{\frac{p+1}{4}}^{-1}\}$, and let $S_p^M \subseteq SO(3)$ denote the set of reduced words of length at most $M = 1, 2, 3, \dots$ in S_p (by reduced we mean all the obvious cancellations such as $\gamma\gamma^{-1}$ have been carried out). We shall verify that

$$|S_p^M| = \frac{p^{M+1} + p^M - p - 1}{p - 1}.$$

Proof.

We prove the fact by induction.

$$\text{For } M = 1, |S_p^1| = \frac{p^2 + p^1 - p - 1}{p - 1} = \frac{p(p-1)}{p-1} = p + 1.$$

Suppose that $|S_p^M| = \frac{p^{M+1} + p^M - p - 1}{p - 1}$. To construct S_p^{M+1} from S_p^M , we multiply the elements of S_p^M of length M by elements of S_p^1 without redundancy. This amounts to adding p new elements to S_p^M . Therefore,

$$|S_p^{M+1}| = p * (|S_p^M| - |S_p^{M-1}|) + |S_p^M|.$$

But,

$$\begin{aligned} p * (|S_p^M| - |S_p^{M-1}|) &= p * \left[\left(\frac{p^{M+1} + p^M - p - 1}{p - 1} \right) - \left(\frac{p^M + p^{M-1} - p - 1}{p - 1} \right) \right] \\ &= \frac{p^{M+2} + p^{M+1} - p^2 - p - p^{M+1} - p^M + p^2 + p}{p - 1} \\ &= \frac{p^{M+2} - p^M}{p - 1}. \end{aligned}$$

Hence,

$$\begin{aligned} |S_p^{M+1}| &= \frac{p^{M+2} - p^M}{p-1} + \frac{p^{M+1} + p^M - p - 1}{p-1} \\ &= \frac{p^{M+2} + p^{M+1} - p - 1}{p-1}. \end{aligned}$$

Consequently, the fact is proven. \square

Theorem 3.2 [L-P-S].

$$\left\| \frac{1}{|S_p^M|} T_{S_p^M} - P_{\mathcal{H}_0} \right\| \leq \text{const} \frac{\log(|S_p^M|)}{\sqrt{|S_p^M|}}.$$

Example 3.3. For $p = 5$, the construction can be described quite concisely.

$S_5 = \{A, B, C, A^{-1}, B^{-1}, C^{-1}\}$, where A, B, C are rotations about the $X,$

$Y,$ and Z axes, each through an angle of $\arccos(-\frac{3}{5})$. So $|S_5^M| = \frac{3}{2}(5^M - 1)$.

$S_5^M = \{A, B, C, A^{-1}, B^{-1}, C^{-1}, AA, AB, AC, AB^{-1}, AC^{-1}, \dots\}$. The set S_5^M contains $\frac{3}{2}(5^M - 1)$ elements of rotations.

This construction is just the simplest one from an infinite family; for each prime p congruent to 1 modulo 4, there is a construction involving $p + 1$ generator rotations, which corresponds to ways of writing p as the sum of four squares of integers with the first addend being positive and odd [L-P-S].

Chapter 4

Equidistribution on the Unit Sphere

Of practical importance is the problem of generating equidistributed points on the sphere. The problem of generating a large number of points on the sphere has many applications in various fields of computation such as quadrature, placing grids on S^2 , tomography, coding theory, etc. See [Sl], [C], and [T], for example.

The advantage of an equidistributed points system lies in the fact that relatively few samplings of the data are needed, and approximate integration can be performed by computation of a mean value, i.e. the arithmetical mean.

4.1 Equidistribution via a Ramanujan set of rotations

We will use the set S_5^M discussed in Example 3.3 to generate points on the unit sphere. A stereographic projection can be used to relate points in the complex plane \mathbb{C} to points on the sphere. To every point $\xi = (\xi_1, \xi_2, \xi_3)^T$ on the unit sphere, except the north pole $(0, 0, 1)^T$, we associate a complex number

$$z = \frac{\xi_1 + i\xi_2}{1 - \xi_3}.$$

Under this stereographic projection the fractional linear transformations in

the complex plane correspond to rotations on the sphere. Taking this into account, it is convenient to actually compute with points in \mathbb{C} and to use fractional transformations instead of rotations. The A, B, C correspond to the linear fractional transformations defined by the matrices:

$$A_p = \frac{1}{\sqrt{5}} \begin{pmatrix} 1+2i & 0 \\ 0 & 1-2i \end{pmatrix}, B_p = \frac{1}{\sqrt{5}} \begin{pmatrix} 1 & 2 \\ -2 & 1 \end{pmatrix}, C_p = \frac{1}{\sqrt{5}} \begin{pmatrix} 1 & 2i \\ 2i & 1 \end{pmatrix}.$$

The process of projecting our points onto the complex plane and then pulling them back to the unit sphere goes as follows:

Let $\xi = (\xi_1, \xi_2, \xi_3)^T$ be a point on the unit sphere, except the north pole $(0, 0, 1)^T$. We associate to it by means of the stereographic projection

$$z = \frac{\xi_1 + i\xi_2}{1 - \xi_3}.$$

The rotation group $SO(3)$ is mapped onto $SU(2)$, with homographic action on \mathbb{C} :

$$z \rightarrow \frac{az + b}{cz + d}, \quad \begin{pmatrix} a & b \\ c & d \end{pmatrix} \in SU(2).$$

So z transforms to \bar{z} as

$$\bar{z} = \frac{az + b}{cz + d}.$$

The final step in the process is to project \bar{z} back to the unit sphere via the inverse stereographic projection.

We get then the rotated point $\tilde{\xi} = (\tilde{\xi}_1, \tilde{\xi}_2, \tilde{\xi}_3)^T$ where

$$(\tilde{\xi}_1, \tilde{\xi}_2, \tilde{\xi}_3)^T = \left(\frac{2\Re(\bar{z})}{1 + |\bar{z}|^2}, \frac{2\Im(\bar{z})}{1 + |\bar{z}|^2}, \frac{|\bar{z}|^2 - 1}{1 + |\bar{z}|^2} \right).$$

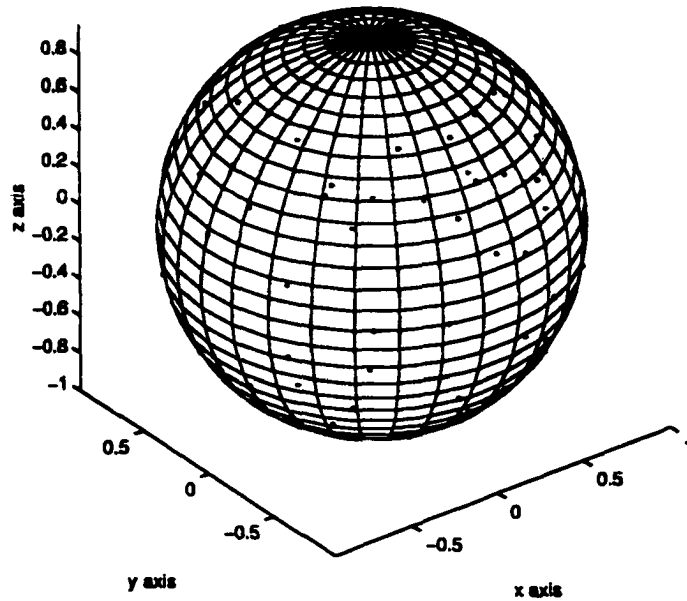


FIGURE 1. 200 points generated using S_5^M

In order to visualize the distribution of the points on the sphere, we made sample plots of these points for the initial point $(\frac{1}{\sqrt{3}}, \frac{1}{\sqrt{3}}, \frac{1}{\sqrt{3}}) \in S^2$. Using the stereographic projection, this point corresponds to $\frac{1+i}{\sqrt{3}} \in \mathbb{C}$.

If the initial point lies on one of the coordinate axes, then the resulting distribution of points displays an undesirable amount of symmetry. Therefore, we need to fix a starting point $p \in S^2$ lying on none of the coordinate axes.

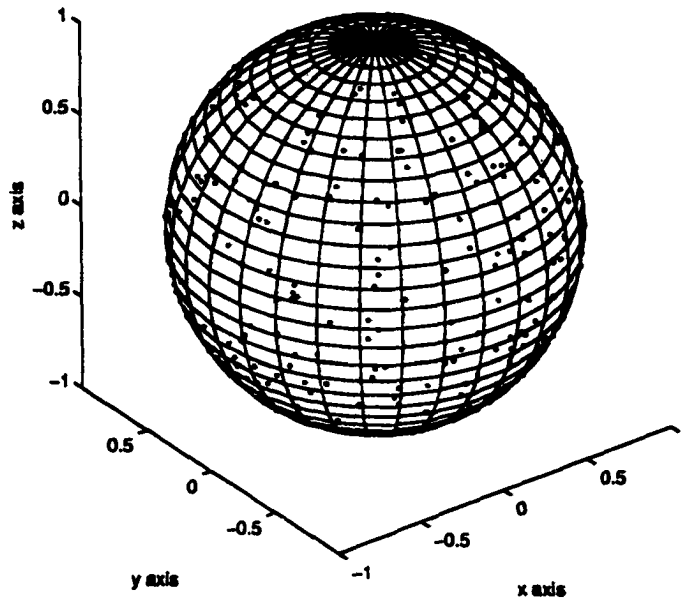


FIGURE 2. 1000 points generated using S_5^M

Theorem 3.2 gives the quadrature error bound for the Ramanujan set and it is near-optimal for the numerical integration of functions on S^2 , as we will see in the next two examples.

4.2 Numerical results

Example 4.2.1.

We discuss the integration of a discontinuous function, namely the characteristic function given by

$$\chi_h(\xi \cdot \xi_0) = \begin{cases} 1 & \text{if } h \leq \xi \cdot \xi_0 \leq 1, \\ 0 & \text{elsewhere} \end{cases}$$

for fixed $\xi_0 \in S^2$.

The exact value of the integral is the area of the spherical cap (the intersection of S^2 with half spaces) of radius $1 - h$, so

$$\int_{S^2} \chi_h(\xi \cdot \xi_0) d\omega(\xi) = 2\pi(1 - h).$$

To test our distribution, we choose different values for h and $\xi_0 = (\frac{1}{\sqrt{3}}, \frac{1}{\sqrt{3}}, \frac{1}{\sqrt{3}})^T$.

Using the Ramanujan set of rotations S_5^M to approximate the integral, we have

$$\frac{1}{|S_5^M|} \sum_{\gamma \in S_5^M} \chi_h(\gamma \xi \cdot \xi_0) \approx \frac{1}{4\pi} \int_{S^2} \chi_h(\xi \cdot \xi_0) d\omega(\xi) = \frac{1 - h}{2}.$$

No. of points	$h = 0.95$	$h = 0.8$	$h = 0.5$
50	0.02	0.08	0.18
100	0.02	0.14	0.19
150	0.02	0.14	0.1933
200	0.02	0.15	0.19
250	0.02	0.152	0.184
300	0.0233	0.15	0.1933
350	0.0229	0.14	0.1971
400	0.025	0.1425	0.205
Exact value	0.025	0.1	0.25

TABLE 1. Example 1

Table 1 gives an impression of the numerical results. The smaller the radius $1 - h$ is, the better results we get. Even though the function is discontinuous, we are getting acceptable results using only a few generated points.

This example deals with the integration of the function

$$\int_{S^2} \cos(\xi \cdot r\xi_0) d\omega(\xi) = 4\pi \frac{\sin(r)}{r}.$$

Using the set S_5^M we approximate the integral by

$$\frac{1}{|S_5^M|} \sum_{\gamma \in S_5^M} \cos(\gamma\xi \cdot r\xi_0) \approx \frac{1}{4\pi} \int_{S^2} \cos(\xi \cdot r\xi_0) d\omega(\xi) = \frac{\sin(r)}{r}.$$

For the numerical tests, we take three different values for r and $\xi_0 = (0, 0, 1)^T$.

Table 2 shows the results. The function is smooth for small r and that explains the good results for $r = 0.1$.

No. of points	$r = 1$	$r = .5$	$r = .1$
50	0.8419	0.9587	0.9983
100	0.8548	0.9622	0.9985
150	0.8509	0.9612	0.9984
200	0.8477	0.9603	0.9984
250	0.8487	0.9609	0.9984
300	0.852	0.9609	0.9984
Exact value	0.8415	0.9567	0.9983

TABLE 2. Example 2

Chapter 5

Covering of the Sphere

The material that follows had as its inspiration two sources. One is the fact that covering the unit sphere with n spherical caps that possess the smallest possible radius is still a challenging and unsolved problem. The centers of such an extremal system of caps are then the positions for the n fuel depots that may be placed on any spherical planet so that the distance of any point on the surface from the nearest depot is as small as possible.

The other source for thinking about covering the unit sphere with spherical caps of radius h is the multiresolution analysis on S^2 , especially if one wants to have a nested sequence of covers with a specific radius.

This led to the investigation of the general question: how many spherical caps of radius h do we need to cover the unit sphere? We are looking for an explicit formula for the number of spherical caps needed and an exact positioning of the centers of the spherical caps that cover the whole unit sphere without giving any preferences to any region on the sphere.

We will use in this dissertation the Ramanujan set of rotations only in the case when $p = 5$. Let $A \subseteq S^2$ be a spherical cap with center $y \in S^2$ and radius h .

The area $|A| = 2\pi h$. Denote by χ_A the characteristic function of A . In

order for the set $\{\gamma A\}_{\gamma \in S_5^M}$ to cover the whole unit sphere, one has to make sure that for every $x \in S^2$, there exists at least one spherical cap, say γA , where $\gamma \in S_5^M$, such that $x \in \gamma A$.

Theorem 5.1. *Let $C_M = 5^{\frac{M}{2}}(M + 1 + \frac{M}{\sqrt{5}})$, and let $k = 4^{\frac{(16+\sqrt{\pi})}{\pi}}$. Then, for every cap $A \subseteq S^2$ and for all $x \in S^2$ we have*

$$\left| |A| - \frac{1}{|S_5^M|} \sum_{\gamma \in S_5^M} \chi_{\gamma A}(x) \right| \leq \frac{3}{4^{\frac{1}{2}}} (4\pi)^{\frac{1}{2}} \left[\frac{C_M}{|S_5^M|} k \right]^{\frac{2}{3}} \quad (5.1)$$

Proof. Here we follow an argument in [L-P-S] making it more precise at various points.

Let $A \subseteq S^2$ be a spherical cap with center $y \in S^2$ and radius h . The area $|A| = 2\pi h$. Denote by χ_A the characteristic function of A . Let A_1, A_2 be two spherical caps about y with the radii $h - 2\varepsilon$ and $h + 2\varepsilon$, respectively. Therefore, $|A_1| = 2\pi(h - 2\varepsilon)$, and $|A_2| = 2\pi(h + 2\varepsilon)$. We have

$$||A_\nu| - |A|| = 2\pi |(h \pm 2\varepsilon) - h| = 4\pi\varepsilon, \quad (\nu = 1, 2).$$

For $\varepsilon > 0$ let $k_\varepsilon(z, \xi)$ be the point-pair invariant

$$k_\varepsilon(z, \xi) = \begin{cases} \frac{1}{2\pi(1 - \cos(\varepsilon))} & \text{if } d(z, \xi) < \varepsilon, \\ 0 & \text{otherwise.} \end{cases}$$

Define $k * f(z)$ by

$$k * f(z) = \int_{S^2} k(z, \xi) f(\xi) dx.$$

We get

$$\begin{aligned} \left| \frac{1}{|S_5^M|} \sum_{\gamma \in S_5^M} (\chi_{A_\nu} * k_\epsilon)(\gamma x) - |A| \right| &\leq \left| \frac{1}{|S_5^M|} \sum_{\gamma \in S_5^M} (\chi_{A_\nu} * k_\epsilon)(\gamma x) - |A_\nu| \right| + \left| |A_\nu| - |A| \right| \\ &\leq \left| \frac{1}{|S_5^M|} \sum_{\gamma \in S_5^M} (\chi_{A_\nu} * k_\epsilon)(\gamma x) - |A_\nu| \right| + 4\pi\epsilon. \end{aligned}$$

Let

$$I_\nu = \left| \sum_{\gamma \in S_5^M} (\chi_{A_\nu} * k_\epsilon)(\gamma x) - |S_5^M| |A_\nu| \right|.$$

Then

$$\left| \frac{1}{|S_5^M|} \sum_{\gamma \in S_5^M} (\chi_{A_\nu} * k_\epsilon)(\gamma x) - |A| \right| \leq \frac{1}{|S_5^M|} I_\nu + 4\pi\epsilon. \quad (5.2)$$

The Legendre polynomials $P_n(x)$ are defined as

$$P_n(x) = \frac{1}{2^n n!} \frac{d^n}{dx^n} (x^2 - 1)^n.$$

Also $P_n(1) = 1$ and

$$\int_{-1}^1 P_m(x) P_n(x) dx = \frac{2}{2n+1} \delta_{m,n}.$$

Now, we need to estimate I_ν . By (2.9) in [L-P-S], we have

$$I_\nu = \left| \sum_{m=1}^{\infty} \hat{k}_\epsilon(m) \hat{k}_{A_\nu}(m) \sum_{|j| \leq m} \varphi_{j,m}(y) \sum_{\gamma \in S_5^M} \varphi_{j,m}(\gamma x) \right|$$

where $\hat{k}_{A_\nu}(m) = 2\pi \int_{\cos \rho_\nu}^1 P_m(x) dx$ and $\hat{k}_\epsilon(m) = \frac{1}{1 - \cos \epsilon} \int_{\cos \epsilon}^1 P_m(x) dx$. Fur-

thermore, the $\varphi_{j,m}$ are simultaneous eigenvectors for the averaging operator

T_S , and for the operator defined by k_ϵ . We now use the inequality (see [L-P-S], page 161)

$$\left| \sum_{\gamma \in S_\epsilon^M} \varphi_{j,m}(\gamma x) \right| \leq C_M |\varphi_{j,m}(x)|.$$

Therefore,

$$I_\nu \leq C_N \sum_{m=1}^{\infty} \left| \hat{k}_\epsilon(m) \hat{k}_{A_\nu}(m) \right| \sum_{|j| \leq m} |\varphi_{j,m}(x) \varphi_{j,m}(y)|.$$

By the Cauchy-Schwartz inequality, we obtain

$$\sum_{|j| \leq m} |\varphi_{j,m}(x) \varphi_{j,m}(y)| \leq \left(\sum_{|j| \leq m} |\varphi_{j,m}(x)|^2 \right)^{\frac{1}{2}} \left(\sum_{|j| \leq m} |\varphi_{j,m}(y)|^2 \right)^{\frac{1}{2}}.$$

Furthermore,

$$\sum_{|j| \leq m} |\varphi_{j,m}(z)|^2 = \frac{2m+1}{2\pi} \quad \text{for all } z \in S^2.$$

Consequently,

$$I_\nu \leq C_N \sum_{m=1}^{\infty} \left| \hat{k}_\epsilon(m) \hat{k}_{A_\nu}(m) \right| \frac{2m+1}{2\pi}.$$

The next step in the proof is to bound $\hat{k}_{A_\nu}(m)$ and $\hat{k}_\epsilon(m)$ from above. Recall that

$$(2m+1)P_m(x) = P'_{m+1}(x) - P'_{m-1}(x).$$

Using the above equation, $\hat{k}_{A_\nu}(m)$ and $\hat{k}_\epsilon(m)$ can be rewritten as

$$\begin{aligned} \hat{k}_{A_\nu}(m) &= \frac{2\pi}{2m+1} [P_{m+1}(\cos \rho_\nu) - P_{m-1}(\cos \rho_\nu)] \\ \hat{k}_\epsilon(m) &= \frac{1}{(2m+1)(1-\cos \epsilon)} [P_{m+1}(\cos \epsilon) - P_{m-1}(\cos \epsilon)]. \end{aligned}$$

To bound $\hat{k}_{A_\nu}(m)$ and $\hat{k}_\epsilon(m)$ from above, we need the following lemma.

Lemma 5.2. For $0 \leq \theta \leq \pi$, we have the following inequality

$$|P_{m-1}(\cos(\theta)) - P_{m+1}(\cos(\theta))| \leq \frac{8}{\sqrt{\pi}} \sqrt{\frac{|\sin(\theta)|}{m}}.$$

Proof. Recall a result of Stieltjes ([Sz], Theorem 7.33, page 165)

$$\sqrt{\sin(\theta)} |P_n(\cos(\theta))| \leq \sqrt{\frac{2}{\pi}} \frac{1}{\sqrt{n}} \quad (0 \leq \theta \leq \pi). \quad (5.3)$$

Bernstein's theorem ([Sz], Theorem 1.22.1, page 5) states that for any trigonometric polynomial $g(\theta)$ of degree n , we have

$$|g'(\theta)| \leq n \cdot \max_{0 \leq \theta_1 \leq 2\pi} |g(\theta_1)| \quad (0 \leq \theta \leq 2\pi). \quad (5.4)$$

Let $0 \leq \theta_0 \leq \frac{\pi}{2}$. We see from (5.3) that

$$|P_n(\cos(\theta))| \leq \sqrt{\frac{2}{\pi}} \frac{1}{\sqrt{n}} \frac{1}{\sqrt{\sin(\theta)}} \leq \sqrt{\frac{2}{\pi}} \frac{1}{\sqrt{n}} \frac{1}{\sqrt{\sin(\theta_0)}} \quad (\theta_0 \leq \theta \leq \frac{\pi}{2}). \quad (5.5)$$

Let $\cos(\theta) = \cos(\theta_0) \cos(u)$. Then by (5.5) for all real u

$$|P_n(\cos(\theta_0) \cos(u))| \leq \sqrt{\frac{2}{\pi}} \frac{1}{\sqrt{n}} \frac{1}{\sqrt{\sin(\theta_0)}}. \quad (5.6)$$

Hence, (5.4) and (5.6) imply

$$|\cos(\theta_0) \sin(u) P_n'(\cos(\theta_0) \cos(u))| \leq \sqrt{\frac{2}{\pi}} \frac{\sqrt{n}}{\sqrt{\sin(\theta_0)}}. \quad (5.7)$$

Equivalently, for $\theta_0 \leq \theta \leq \frac{\pi}{2}$,

$$\sqrt{\cos^2(\theta_0) - \cos^2(\theta)} \cdot |P_n'(\cos(\theta))| \leq \sqrt{\frac{2}{\pi}} \frac{\sqrt{n}}{\sqrt{\sin(\theta_0)}}. \quad (5.8)$$

Given $0 \leq \gamma \leq \frac{\pi}{2}$ set $\theta_0 = \frac{\gamma}{2}$, $\theta = \gamma$. Then (5.8) implies

$$|P'_n(\cos(\gamma))| \leq \sqrt{\frac{2}{\pi}} \frac{\sqrt{n}}{\sqrt{\cos^2(\frac{\gamma}{2}) - \cos^2(\gamma)}} \frac{1}{\sqrt{\sin(\frac{\gamma}{2})}}. \quad (5.9)$$

But

$$\cos^2(\frac{\gamma}{2}) - \cos^2(\gamma) = \sin^2(\gamma) - \sin^2(\frac{\gamma}{2}) = \sin^2(\frac{\gamma}{2})(4 \cos^2(\frac{\gamma}{2}) - 1) \geq \sin^2(\frac{\gamma}{2}).$$

Hence, by (5.9),

$$|P'_n(\cos(\gamma))| \leq \sqrt{\frac{2}{\pi}} \frac{\sqrt{n}}{(\sin(\frac{\gamma}{2}))^{\frac{3}{2}}}. \quad (5.10)$$

From ([Sz], (1), page 360) we have

$$P_{n-1}(x) - P_{n+1}(x) = \frac{2n+1}{n(n+1)}(1-x^2)P'_n(x). \quad (5.11)$$

By combining (5.10) and (5.11) we get

$$\begin{aligned} |P_{n-1}(\cos(\gamma)) - P_{n+1}(\cos(\gamma))| &\leq \frac{2n+1}{n(n+1)} \sin^2(\gamma) \sqrt{\frac{2}{\pi}} \frac{\sqrt{n}}{(\sin(\frac{\gamma}{2}))^{\frac{3}{2}}} \\ &= \frac{2n+1}{n+1} \frac{1}{\sqrt{n}} \sqrt{\frac{2}{\pi}} \frac{\sin^2(\gamma)}{(\sin(\frac{\gamma}{2}))^{\frac{3}{2}}}. \end{aligned}$$

But

$$\sin(\gamma) = 2 \sin(\frac{\gamma}{2}) \cos(\frac{\gamma}{2}).$$

So

$$\frac{1}{\sin(\frac{\gamma}{2})} = \frac{2 \cos(\frac{\gamma}{2})}{\sin(\gamma)} \leq \frac{2}{\sin(\gamma)}.$$

Therefore

$$|P_{n-1}(\cos(\gamma)) - P_{n+1}(\cos(\gamma))| \leq 4 \frac{2n+1}{n+1} \frac{1}{\sqrt{n}} \frac{1}{\sqrt{\pi}} \sqrt{\sin(\gamma)}. \quad (5.12)$$

Consequently, for $0 \leq \gamma \leq \frac{\pi}{2}$,

$$|P_{n-1}(\cos(\gamma)) - P_{n+1}(\cos(\gamma))| \leq \frac{8}{\sqrt{\pi}} \sqrt{\frac{|\sin(\gamma)|}{n}}. \quad (5.13)$$

Hence, the lemma is proven. \square

Using the previous lemma and setting $t = \frac{8}{\sqrt{\pi}}$, we have the following inequalities

$$|\hat{k}_{A_\nu}(m)| \leq \frac{2\pi}{2m+1} t \sqrt{\frac{|\sin(\rho_\nu)|}{m}} \leq \frac{2\pi t}{(2m+1)\sqrt{m}}.$$

Similarly

$$|\hat{k}_\varepsilon(m)| \leq \frac{1}{(2m+1)(1-\cos(\varepsilon))} t \frac{\sqrt{\sin(\varepsilon)}}{\sqrt{m}}.$$

Also, $|\hat{k}_\varepsilon(m)| \leq 1$ for all m , to conclude that

$$\begin{aligned} I_\nu &\leq C_M \sum_{1 \leq m \leq \frac{1}{\varepsilon}} |\hat{k}_\varepsilon(m) \hat{k}_{A_\nu}(m)| \frac{2m+1}{2\pi} + C_M \sum_{m > \frac{1}{\varepsilon}} |\hat{k}_\varepsilon(m) \hat{k}_{A_\nu}(m)| \frac{2m+1}{2\pi} \\ &\leq C_M \left[\sum_{1 \leq m \leq \frac{1}{\varepsilon}} \frac{t}{\sqrt{m}} + \sum_{m > \frac{1}{\varepsilon}} \frac{t^2 \sqrt{\sin(\varepsilon)}}{(1-\cos(\varepsilon))} \frac{1}{(2m+1)m} \right] \\ &= C_M t \left[\sum_{1 \leq m \leq \frac{1}{\varepsilon}} \frac{1}{\sqrt{m}} + t \frac{\sqrt{\sin(\varepsilon)}}{(1-\cos(\varepsilon))} \sum_{m > \frac{1}{\varepsilon}} \frac{1}{(2m+1)m} \right]. \end{aligned}$$

Notice that for the first part of the sum we have

$$\sum_{1 \leq m \leq \frac{1}{\varepsilon}} \frac{1}{\sqrt{m}} \leq \int_0^{\frac{1}{\varepsilon}} \frac{1}{\sqrt{x}} dx = \frac{1}{2} \frac{1}{\sqrt{\varepsilon}}.$$

Furthermore, for the second part we have the following two inequalities:

$$\frac{\sqrt{\sin(\varepsilon)}}{(1-\cos(\varepsilon))} \leq \frac{\sqrt{\varepsilon}}{\frac{\varepsilon^2}{2}} = 2 \frac{1}{\varepsilon^{\frac{3}{2}}}$$

$$\sum_{m > \frac{1}{\varepsilon}} \frac{1}{(2m+1)m} \leq \frac{1}{2} \sum_{m > \frac{1}{\varepsilon}} \frac{1}{m^2} \leq \frac{1}{2} \int_{(\frac{1}{\varepsilon})-1}^{\infty} \frac{1}{x^2} dx = \frac{1}{2} \frac{1}{\frac{1}{\varepsilon} - 1} \leq \frac{\varepsilon}{2}.$$

Hence,

$$I_\nu \leq C_M t \left[\frac{1}{2} \frac{1}{\sqrt{\varepsilon}} + 2t \frac{1}{\varepsilon^{\frac{3}{2}}} \frac{\varepsilon}{2} \right] = C_M t \left(\frac{1}{2} + t \right) \frac{1}{\sqrt{\varepsilon}}. \quad (5.14)$$

By combining (5.14) with (5.2) we get

$$\left| \frac{1}{|S_5^M|} \sum_{\gamma \in S_5^M} (\chi_{A_\nu} * k_\varepsilon)(\gamma x) - |A| \right| \leq \frac{C_M}{|S_5^M|} t \left(\frac{1}{2} + t \right) \frac{1}{\sqrt{\varepsilon}} + 4\pi\varepsilon.$$

Set $k = t \left(\frac{1}{2} + t \right) = 4 \frac{(16 + \sqrt{\pi})}{\pi}$. It is easy to verify that, for any $x_1, \dots, x_n \in S^2$,

we have

$$\sum_{r=1}^n (\chi_{A_1} * k_\varepsilon)(x_r) \leq \sum_{r=1}^n \chi_A(x_r) \leq \sum_{r=1}^n (\chi_{A_2} * k_\varepsilon)(x_r).$$

In conclusion,

$$\left| |A| - \frac{1}{|S_5^M|} \sum_{\gamma \in S_5^M} \chi_A(\gamma x) \right| \leq \frac{C_M}{|S_5^M|} k \frac{1}{\sqrt{\varepsilon}} + 4\pi\varepsilon.$$

The previous inequality is valid for every ε , such that $0 < \varepsilon < 1$, so the following inequality

$$\left| |A| - \frac{1}{|S_5^M|} \sum_{\gamma \in S_5^M} \chi_A(\gamma x) \right| \leq \min_{0 < \varepsilon < 1} \left(\frac{C_M}{|S_5^M|} k \frac{1}{\sqrt{\varepsilon}} + 4\pi\varepsilon \right) \quad (5.15)$$

still holds.

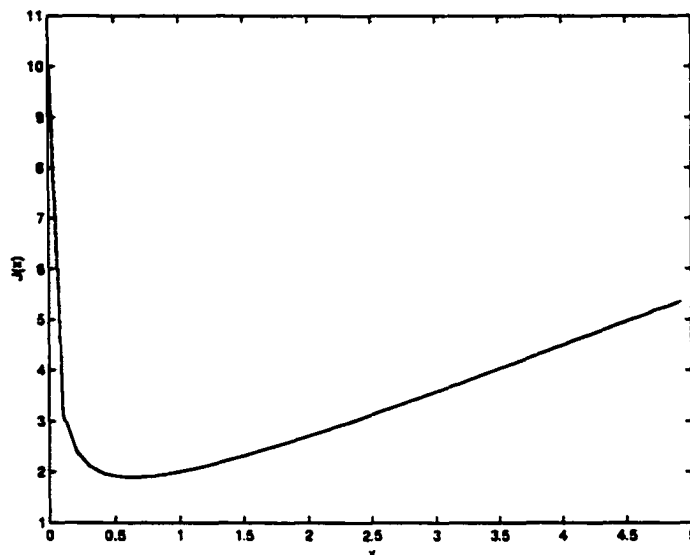


FIGURE 3. The graph of $J(x)$ for $k_1 = 1$ and $k_2 = 1$

Lemma 5.3.

$$\min_{0 < \varepsilon < 1} \left(\frac{C_M}{|S_5^M|} k \frac{1}{\sqrt{\varepsilon}} + 4\pi\varepsilon \right) = \frac{3}{4^{\frac{1}{3}}} (4\pi)^{\frac{2}{3}} \left[\frac{C_M}{|S_5^M|} k \right]^{\frac{2}{3}}.$$

Proof. Let $J(\varepsilon) = k_1\varepsilon + \frac{k_2}{\sqrt{\varepsilon}}$, where $\varepsilon > 0$. The graph of $J(\varepsilon)$ is shown in figure 3. The minimum of $J(\varepsilon)$ occurs at $\varepsilon_0 = \left(\frac{k_2}{2k_1}\right)^{\frac{2}{3}}$, and $\min J(\varepsilon) = J(\varepsilon_0) = \frac{3}{4^{\frac{1}{3}}} k_1^{\frac{1}{3}} k_2^{\frac{2}{3}}$. In our case, $k_1 = 4\pi$ and $k_2 = \frac{C_M}{|S_5^M|} k$. Therefore, the lemma follows. \square

Combining (5.15) and Lemma 5.3, Theorem 5.1 is proven. \square

Furthermore, in order to use Theorem 5.1 to guarantee the covering of the sphere, we need the following Lemma 5.4.

Lemma 5.4.

$$\left| |A| - \frac{1}{|S_5^M|} \sum_{\gamma \in S_5^M} \chi_{\gamma A}(x) \right| < |A| \Rightarrow \bigcup_{\gamma \in S_5^M} \gamma A = S^2.$$

Proof. As $\gamma A \subseteq S^2$, then $\bigcup_{\gamma \in S_5^M} \gamma A \subseteq S^2$. Now, letting $x \in S^2$ we have

$$\left| |A| - \frac{1}{|S_5^M|} \sum_{\gamma \in S_5^M} \chi_{\gamma A}(x) \right| < |A| \Rightarrow \sum_{\gamma \in S_5^M} \chi_{\gamma A}(x) \neq 0.$$

So, we can see that there exists a $\gamma \in S_5^M$ such that $\chi_{\gamma A}(x) = 1$. This is equivalent to saying that $x \in \gamma A$. As $\gamma A \subseteq \bigcup_{\gamma \in S_5^M} \gamma A$, the lemma follows. \square

Based on this fact and on Theorem 5.1, we reach a covering if

$$\frac{3}{4^{\frac{1}{3}}}(4\pi)^{\frac{1}{3}} \left[\frac{5^{\frac{M}{2}}(M+1+\frac{M}{\sqrt{5}})}{|S_5^M|} 4\left(\frac{16+\sqrt{\pi}}{\pi}\right) \right]^{\frac{2}{3}} < 2\pi h. \quad (5.16)$$

As $n = \frac{3}{2}(5^M - 1)$, then $M = \log_5(\frac{2n}{3} + 1)$, and $5^{\frac{M}{2}} = \sqrt{\frac{2}{3}n + 1}$. Inequality

(5.16) can be simplified as follows

$$\frac{\sqrt{\frac{2}{3}n + 1} \left[1 + \left(1 + \frac{1}{\sqrt{5}}\right) \log_5\left(\frac{2n}{3} + 1\right) \right]}{n} < \frac{1}{6} \sqrt{\frac{2}{3}} \frac{\pi^2}{16 + \sqrt{\pi}} h^{\frac{2}{3}}. \quad (5.17)$$

The left hand side of (5.17) is less than

$$\frac{\sqrt{2} \sqrt{\frac{2}{3}} \sqrt{n} 2\left(1 + \frac{1}{\sqrt{5}}\right) \log_5 n}{n}$$

and so we have proven the following Proposition 5.5.

Proposition 5.5.

If n satisfies the following inequality

$$\frac{\log n}{\sqrt{n}} < \frac{\sqrt{5}(\log 5)\pi^2}{12\sqrt{2}(\sqrt{5}+1)(16+\sqrt{\pi})} h^{\frac{3}{2}}$$

then the sphere covering

$$\bigcup_{\gamma \in S^M} \gamma A = S^2.$$

is guaranteed.

Chapter 6

One Dimensional Wavelets

Digital signal processing requires mathematical tools to transform multi-frequency (multiresolutional) time-varying signals for data compression, pattern recognition, and digital filtering.

Domain transforms such as the Fast Fourier Transform (FFT) and the Discrete Cosine Transforms (DCT) had been at the forefront of signal transformation and analysis until the introduction of the wavelet transform in the early 1980s.

Wavelet theory involves representing general functions in terms of simpler, fixed building blocks at different scales and positions. This has been found to be a useful approach in several different areas.

In the early 80's, Strömberg discovered the first continuous orthogonal wavelets [St]. This was done in the context of trying to further understand Hardy spaces, as well as other spaces used to measure the size and smoothness of functions. And long before this were results by Haar [Ha], Franklin [F], and others.

Lemarié and Meyer [L-M], independent of Strömberg, constructed new orthogonal wavelet expansions. With the notion of multiresolution analysis, introduced by Mallat and Meyer, a systematic framework for understanding

these orthogonal expansions was developed [M]. It also provided the connection with quadrature mirror filtering. Daubechies [Da] gave a construction of wavelets, nonzero only on a finite interval and with arbitrarily high, but fixed, regularity.

Unlike the Fourier transform, which decomposes a signal into component frequencies, a wavelet transformation uses template matching to choose a waveform closely matching the original signal. The end-result of the process, if not the mechanics, is similar to using look-up table functions. Far fewer terms are required to represent a signal while retaining a high degree of accuracy.

6.1 Wavelets on the real line

Let $L^2(\mathbf{R})$ denote the Hilbert space of complex valued square integrable functions on the real line \mathbf{R} . The scalar product in this space is defined by

$$(f, g) = \int_{\mathbf{R}} f(t)\overline{g(t)} dt \quad (f, g \in L^2(\mathbf{R})). \quad (6.1.1)$$

Definition 6.1.1. *A wavelet is a function $\psi(t) \in L^2(\mathbf{R})$ such that the family of functions*

$$\psi_{j,k} := \sqrt{2^j}\psi(2^j t - k),$$

where j and k are arbitrary integers, is an orthonormal basis in the Hilbert space $L^2(\mathbf{R})$.

A multiresolution of $L^2(\mathbb{R})$ is a sequence V_j , $j \in \mathbb{Z}$, of closed subspaces $V_j \subseteq L^2(\mathbb{R})$, such that

- (a) $f(t)$ belongs to V_0 if and only if $f(t - 1)$ belongs to V_0 ,
- (b) $V_j \subseteq V_{j+1}$ for all $j \in \mathbb{Z}$,
- (c) $f(t)$ belongs to V_j if and only if $f(2t)$ belongs to V_{j+1} for all $j \in \mathbb{Z}$,
- (d) $\bigcap_{j=-\infty}^{+\infty} V_j = \{0\}$,
- (e) the closure of $\bigcup_{j=-\infty}^{+\infty} V_j = L^2(\mathbb{R})$,
- (f) there is a function $\phi \in V_0$, such that the set

$$\{\phi(t - k)\}, \quad k \in \mathbb{Z}, \quad \text{is an orthonormal basis of } V_0. \quad (6.1.2)$$

The function ϕ is usually called the *scaling function*. Clearly the functions

$$\phi_{j,k}(t) = \sqrt{2^j} \phi(2^j t - k) \quad (k \in \mathbb{Z}) \quad (6.1.3)$$

form an orthonormal basis of V_j for each $j \in \mathbb{Z}$.

It will be good to give at this point some interesting examples of multiresolution analyses.

Example 6.1.2. Haar System (1910)

Let $V_j = \{ \text{All functions in } L^2(\mathbb{R}) \text{ constant on all intervals } [k2^{-j}, (k+1)2^{-j}], \text{ for } k \in \mathbb{Z} \}$. And let

$$\phi(t) = \begin{cases} 1 & \text{if } t \in [0, 1), \\ 0 & \text{otherwise.} \end{cases}$$

$\{\phi(t - k)\}_{k \in \mathbf{Z}}$ is an orthonormal basis for V_0 , and $\{V_j\}_{j \in \mathbf{Z}}$ is a multiresolution analysis.

Example 6.1.3. Splines System, due to P. Lemarié and G. Battle.

The vector space V_0 is the set of functions which belong to $C^2 \cap L^2(\mathbf{R})$ and equal to a cubic polynomial on each interval $[k, k + 1]$, $k \in \mathbf{Z}$. It is well known that there exists a unique cubic spline $\phi(t) \in V_0$ such that for every $k \in \mathbf{Z}$

$$\phi(k) = \begin{cases} 1 & \text{if } k=0, \\ 0 & \text{if } k \neq 0. \end{cases}$$

Any function $f(t) \in V_0$ can be decomposed in a unique way,

$$f(t) = \sum_{k=-\infty}^{\infty} c_k \phi(t - k).$$

But, as $\phi(0) = 1$ then $f(k) = c_k$. Therefore $f(t)$ can be written uniquely as

$$f(t) = \sum_{k=-\infty}^{\infty} f(k) \phi(t - k).$$

One can easily show that the sequence of vector spaces $\{V_j\}_{j \in \mathbf{Z}}$ built with property (c) of (6.1.2) is a multiresolution analysis of $L^2(\mathbf{R})$.

Let W_j denote the orthogonal complement of V_j in V_{j+1} , so that for each $j \in \mathbf{Z}$,

$$V_{j+1} = V_j \oplus W_j \quad (6.1.4)$$

is an orthogonal sum decomposition. The main result of the theory of wavelets is that given any multiresolution, there is a function $\psi \in W_0$ such that for each $j \in \mathbf{Z}$, $\{\psi(t - k)\}, k \in \mathbf{Z}$ is an orthonormal basis for W_0 . Moreover,

$$\psi_{j,k}(t) = \sqrt{2^j} \psi(2^j t - k) \quad (k \in \mathbf{Z}) \quad (6.1.5)$$

is an orthonormal basis of W_j . Thus in effect the set

$$\psi_{j,k}(t) = \sqrt{2^j} \psi(2^j t - k) \quad (j, k \in \mathbf{Z}) \quad (6.1.6)$$

is an orthonormal basis of $L^2(\mathbf{R})$.

It has been shown that one can derive a wavelet orthonormal basis from any multiresolution analysis. However, the converse is not true. Let $\psi(t)$ be the function whose Fourier transform is given by

$$\hat{\phi}(\omega) = \begin{cases} 1 & \text{if } \frac{4\pi}{7} \leq |\omega| \leq \pi \text{ or } 4\pi \leq |\omega| \leq 4\pi + \frac{4\pi}{7}, \\ 0 & \text{otherwise.} \end{cases}$$

The translates and dilates

$$(\sqrt{2^j} \psi(2^j t - k))_{(k,j) \in \mathbf{Z}^2}$$

form an orthonormal basis of $L^2(\mathbb{R})$. This counterexample due to Y. Meyer is a wavelet that is not related to any multiresolution analysis.

The beauty of the subject is that the functions ϕ and ψ are completely determined by a single sequence of numbers $h[k]$, $k \in \mathbb{Z}$, which in the most interesting cases has finitely non-zero terms. The relevant relations are the “two-scale dilation equations”:

$$\begin{aligned} \frac{1}{\sqrt{2}}\phi(t) &= \sum_{k=-\infty}^{+\infty} h[k]\phi(2t - k) \\ \frac{1}{\sqrt{2}}\psi(t) &= \sum_{k=-\infty}^{+\infty} g[k]\phi(2t - k) \\ g[k] &= (-1)^{1-k}h[1 - k], \quad k \in \mathbb{Z}. \end{aligned} \tag{6.1.7}$$

The sequences $h[k]$ and $g[k]$, $k \in \mathbb{Z}$, are, respectively, the low-pass filter and the high-pass filter of a two-channel multirate filter bank [Ma], and the function ψ is called a *wavelet*.

Next we process the signal in terms of a given multiresolution. A digital signal is a sequence of real numbers $a_0[k]$, $k \in \mathbb{Z}$, which is identified with a function $f(t)$ in V_0 by the formula:

$$f(t) = \sum_{k=-\infty}^{+\infty} a_0[k]\phi(t - k). \tag{6.1.8}$$

Let the projections of f onto V_{j+1} and onto W_{j+1} be given by

$$\begin{aligned} P_{V_{j+1}} f(t) &= \sum_{k=-\infty}^{+\infty} a_{j+1}[k] \phi_{j+1,k}(t) \\ P_{W_{j+1}} f(t) &= \sum_{k=-\infty}^{+\infty} d_{j+1}[k] \psi_{j+1,k}(t). \end{aligned} \tag{6.1.9}$$

Then the relations between the sequences involved are very simple:

$$\begin{aligned} (a) \quad a_j[p] &= \sum_{k=-\infty}^{+\infty} h[k-2p] a_{j+1}[k], \\ (b) \quad d_j[p] &= \sum_{k=-\infty}^{+\infty} g[k-2p] a_{j+1}[k], \\ (c) \quad a_{j+1}[p] &= \sum_{k=-\infty}^{+\infty} h[p-2k] a_j[k] + \sum_{k=-\infty}^{+\infty} g[p-2k] d_j[k]. \end{aligned} \tag{6.1.10}$$

The first formula (6.1.10.a) describes the projection $V_{j+1} \ni P_{V_{j+1}} f \rightarrow P_{V_j} f \in V_j$. The difference $P_{V_{j+1}} f - P_{V_j} f = P_{W_j} f$ is the “detail” signal described in (6.1.10.b). The formula (6.1.10.c) describes the reconstruction of $P_{V_{j+1}} f$ from $P_{V_j} f$ and $P_{W_j} f$. In the case when the low-pass filter $h[k]$, $k \in \mathbf{Z}$, has finite support, the operations (6.1.10) can be precisely implemented for computation. The computations are relatively simple and can be performed quickly. Given a particular application, one designs an appropriate multiresolution, i.e. chooses the correct filter bank.

Now, we take a look at some important properties of wavelets.

Orthogonality: Orthogonality is convenient to have in many situations, e.g., it directly links the L^2 -norm of a function to the norm of its wavelet

coefficients by

$$\|f\| = \sqrt{\sum_{j,k} c_{j,k}^2}.$$

In the biorthogonal case these two quantities are only equivalent. Another advantage of orthogonal wavelets is that the fast transform is a unitary transformation (i.e., its adjoint is its inverse). Consequently, its condition number is equal to 1, which is the optimal case. This is of importance in numerical calculations. It means that an error present in the initial data will not grow under the transformation, and that stable numerical computations are possible.

Compact support: If the scaling function and wavelet are compactly supported, their corresponding filters H and G are finite impulse response filters, so that the summations in the fast wavelet transform are finite. This obviously is of use in implementations. If they are not compactly supported, a fast decay is desirable so that the filters can be approximated reasonably by finite impulse response filters.

Symmetry: If the scaling function and wavelet are symmetric, then the filters have generalized linear phase. The absence of this property can lead to phase distortion. This is important in signal processing applications.

Smoothness: The smoothness of wavelets plays an important role in compression applications. Compression is usually achieved by setting small co-

efficients $c_{j,k}$ to zero. If the original function represents an image and the wavelet is not smooth, the error can easily be detected visually. Also, a higher degree of smoothness corresponds to better frequency localization of the filters. Finally, smooth basis functions are desired in numerical analysis applications where derivatives are involved.

As could be expected, it is not possible to construct wavelets that have all these properties and there is a trade-off between them.

6.2 Two wavelet-based indices for abrupt changes detection

In this section, we will develop a new method based on the wavelet transform (WT) to detect abrupt changes in non-stationary noisy signals. We will show that the wavelet transform alone or when combined with the short time Fourier transform (STFT) provides a more accurate index of stationarity than the STFT alone (as given in [L-D]), especially for very noisy signals.

One common problem in signal processing is the ability to detect abrupt changes in very short segments of not strictly stationary signals. A method based on time-frequency representations (TFRs) for detecting abrupt spectral changes in noisy signals was recently introduced [L-D]. This paper presents a stationarity index derived from the spectrogram of the signal. They show that the Kolmogorov distance is the best choice for a stationarity index. If

there is no change in the frequency content of the signal the index of stationarity is close to zero, but if a change occurs, then the index of stationarity sharply peaks.

We propose in this section an improvement to this previous method by deriving the stationarity index from the spectrogram of the wavelet coefficients of the signal or from the coefficients themselves rather than from the spectrogram of the signal. We have considered this modification due to the fact that the wavelet transform is a useful tool for non-stationary signal analysis that has found many applications in time-frequency analysis [F1], transient detection [M-H] and speech processing [K-B]. After defining the new modified stationarity indexes, we consider two kinds of signals from [L-D], namely test signals presenting very short frequency-hopped segments and chirp signals corrupted with noise. Comparisons between the original method and the new method are performed for different levels of noise.

The short time Fourier transform (STFT) is most suitable for time-frequency analysis of narrow-band signals whose frequencies are subject to strong but slow time-evolution. However, most of the signals of interest to scientists and engineers, from cardiograms and seismograms to stock market quotations and turbulent velocity fields, do not resemble simple tones and have a much richer structure which often includes the appearance of a wide range

of scales [S-W].

The STFT and the wavelet transform (WT) are subject to the same time-frequency constraint, namely the Heisenberg uncertainty relation

$$\Delta t \cdot \Delta f \geq \frac{1}{4\pi}$$

where Δt and Δf represent uncertainty in both time and frequency. The fundamental difference between these two approaches is how the resolution properties vary throughout the time-frequency plane. There is a classical time and frequency resolution trade-off that underlies the structure of the spectrogram: the choice of an analyzing window of short duration ensures a good time localization, but at the expense of a poor frequency resolution (by Fourier duality), and *vice-versa*. Moreover, once an analyzing window has been chosen, the resolution capabilities of the spectrogram remain fixed for all time and frequency parameters [F-V-R]. One major advantage of the WT is that it has a high frequency resolution at low frequency and a high time resolution at high frequency.

Let U be the signal generated from the wavelets coefficients of the original signal. Denote by $SPEC$ the spectrogram of U . For each time t , two sub-images $SPECI(t; \tau, f)$ and $SPECII(t; \tau, f)$ are extracted from $SPEC$ as follows:

$$SPECI(t; \tau, f) = SPEC(t - w + \tau, f)$$

and

$$SPECII(t; \tau, f) = SPEC(t + \tau, f)$$

where w is the width of the subimages and $\tau \in [0, w]$. After normalizing the obtained subimages, define the modified stationarity index as follows:

$$MSI(t) = \sum_{i=1}^N \sum_{j=1}^M ||SPECI(t; i, j)| - |SPECII(t; i, j)||$$

where $(N, M) = \text{size}(SPECI) = \text{size}(SPECII)$.

The major drawback of the original and the proposed hybrid method is that a spectrogram is used to determine the distances between the subimages. Therefore we consider as a direct method the stationarity index as the wavelet level 1 coefficients of the signal (without invoking the spectrogram of the wavelet transform of the signal).

In all test series, 512 data length signals have been generated via **MATLAB** with a sampling frequency $f_s = 1$ kHz. The signal-to-noise ratio was varied from 0 dB to 6 dB.

A. Test signals generation:

The first series contains signals presenting three frequency-hopped boundaries at time samples 180, 210, and 240 (30 samples per segment). The signal in each segment is composed from a single tone. Let us define a finite tone as $s(f; [t_1, t_2])$, where f is the normalized frequency and $[t_1, t_2]$ the

time duration. Hence, the signals with abrupt changes consist of four tones: $s(0.2; [1, 179])$, $s(0.3; [180, 209])$, $s(0.25; [210, 239])$, and $s(0.2; [240, 512])$. In the second series, finite duration oscillating tones were generated. Define a finite duration oscillating tone as $s(f_c; [t_1, t_2])$, where f_c is the central frequency and $[t_1, t_2]$ the time duration. The signals with abrupt changes consist then in three oscillating tones: $s(0.2; [1, 179])$, $s(0.3; [180, 209])$, $s(0.25; [210, 239])$, and $s(0.2; [240, 512])$.

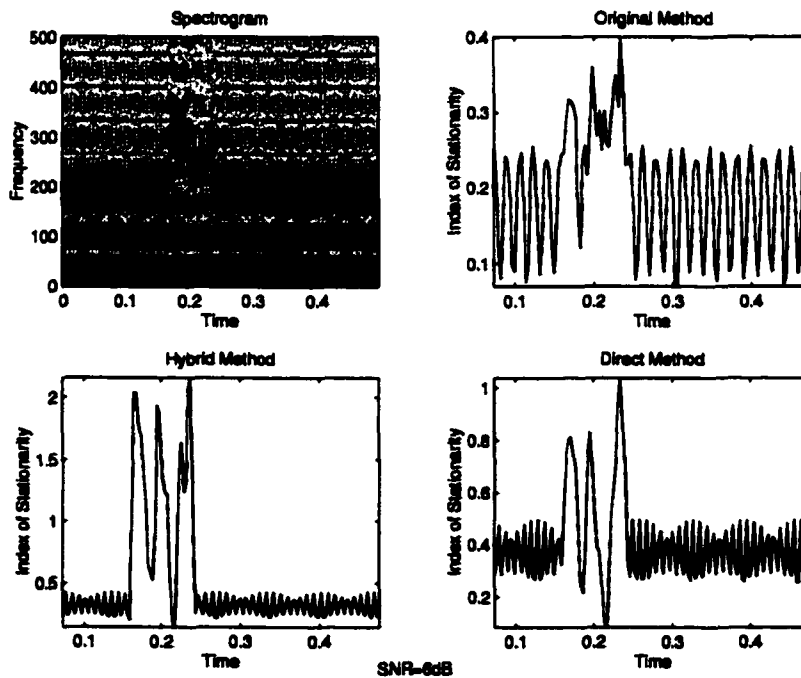


FIGURE 4. Test signals with SNR=6dB and their corresponding stationarity index.

B. Results:

Figure 4 and Figure 5 present the spectrograms of the first series that has the abrupt frequency changes at 0.18, 0.21, and 0.24 with SNR of 6 and 0 dB respectively.

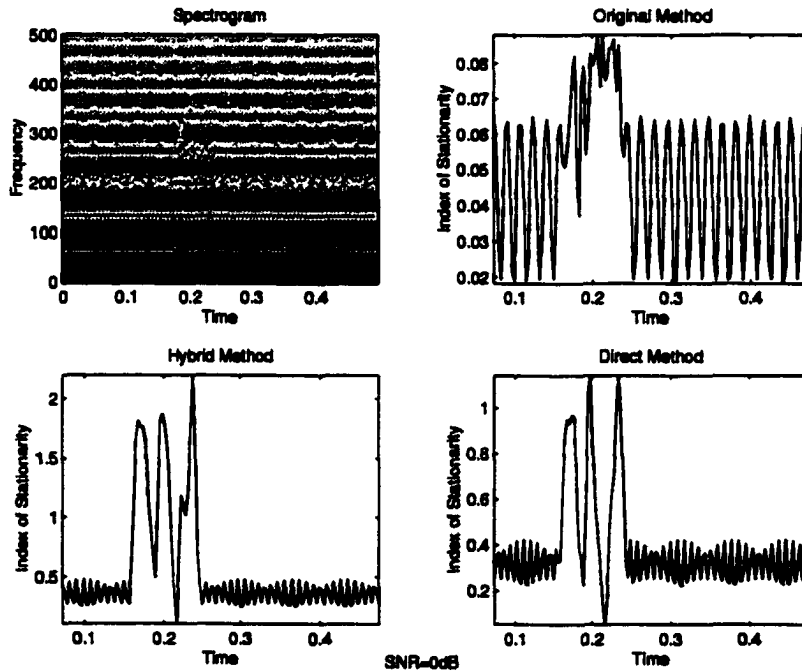


FIGURE 5. Test signals with SNR=0dB and their corresponding stationarity index.

All three methods show good detection and localization of the frequency-hopped times at 6dB SNR. But with 0 dB SNR, the hybrid and the direct method (using the Daubechies-4 wavelets) show a much better ability to

detect the frequency-hops by forming higher peaks in the stationarity index around the time of the abrupt frequency change.

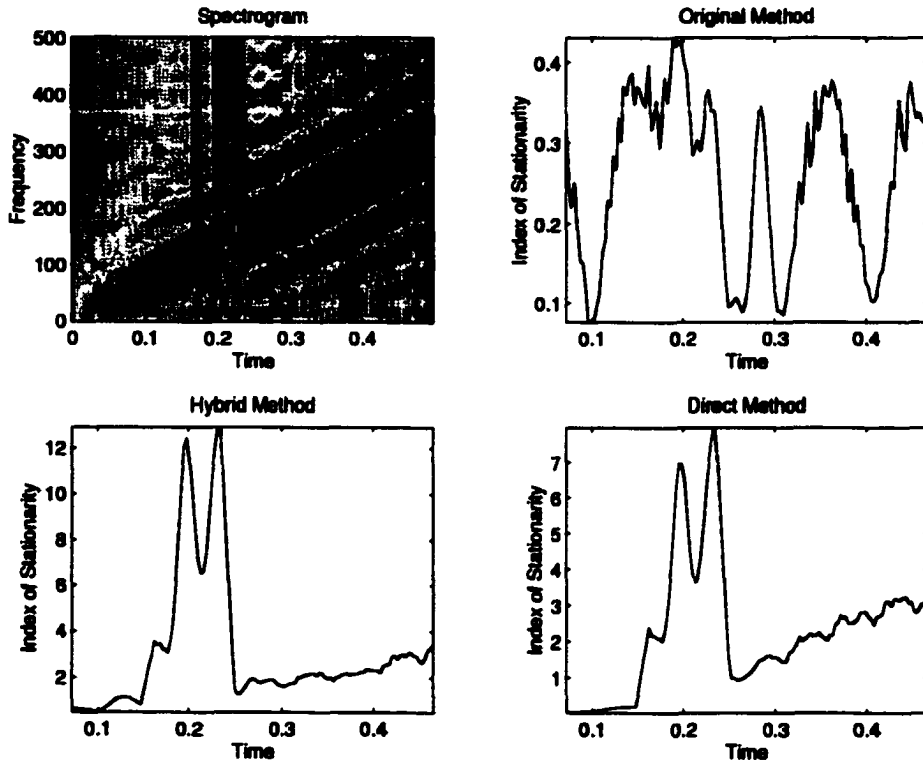


FIGURE 6. Stationarity index of the second series with SNR=0dB.

In the second series, the signals with abrupt changes consist of three oscillating tones. The original method fails to detect the time positions of the sudden changes. In direct contrast, our hybrid and direct methods show peaks in the SI at the times of abrupt changes even with an SNR of 0dB

	Mean 1	Mean 2	Mean 3	Std 1	Std 2	Std 3
Hybrid method	180.5	209.3	240.2	3.9	3.5	3.8
Original method	179.7	209.9	240.2	5.4	5.2	4.6

TABLE 3. Statistical Results: Mean Values and Standard Deviations of the Boundaries Localization {100 records}

(see Figure 6). We observe that the hybrid and direct methods have lower variance than the original method of Laurent and Doncarli.

Chapter 7

Two Dimensional Wavelets

To pass from the one-variable situation to a multivariable situation, we can form tensor products. This is a very general concept which we will use in its most simplest form.

Given n functions of one variable $f^j(x)$ for $j = 1, \dots, n$ we will form the function of n variables $f^1 \otimes f^2 \otimes \dots \otimes f^n = \bigotimes_{j=1}^n f^j$ defined as

$$\bigotimes_{j=1}^n f^j(x_1, \dots, x_n) = \prod_{j=1}^n f^j(x_j).$$

Furthermore, if we have n closed subspaces $X_j \subset L_2(\mathbb{R})$ for $j = 1, 2, \dots, n$ we can form a closed subspace of $L_2(\mathbb{R}^n)$ denoted by $\bigotimes_{j=1}^n X_j$ or by $X_1 \otimes X_2 \otimes \dots \otimes X_n$ and defined as the closed linear span in $L_2(\mathbb{R}^n)$ of all functions of the form $f^1(x_1) \cdot \dots \cdot f^n(x_n)$ where $f^j \in X_j$ for all $j = 1, 2, \dots, n$.

Before we introduce 2D wavelets, let us use the following example as an introduction.

Example 7.1. Two-dimensional Haar wavelet

A natural choice is to use squares in the plane \mathbb{R}^2 . Let V_0 be the space of all functions in $L_2(\mathbb{R}^2)$ which are constant on each square $(n, n+1) \times (k, k+1)$.

When we divide each square into four equal squares we obtain the space V_1 of all functions in $L_2(\mathbb{R}^2)$ which are constant on all squares $(\frac{n}{2}, \frac{n+1}{2}) \times$

$(\frac{k}{2}, \frac{k+1}{2})$. Thus to complement V_0 to V_1 we need three functions on each square $(n, n+1) \times (k, k+1)$. These three orthogonal functions can be given as

$$\psi_1(x, y) = \psi(x) \cdot \phi(y),$$

$$\psi_2(x, y) = \phi(x) \cdot \psi(y),$$

$$\psi_3(x, y) = \psi(x) \cdot \psi(y),$$

where $\psi(x)$ and $\phi(x)$ are respectively the Haar wavelet and scaling function defined in the previous chapter. Clearly these functions are in V_1 . The functions $\psi_j(x-k, y-l)$ for all $k, l \in \mathbf{Z}$ and $j = 1, 2, 3$ form an orthonormal system.

We will follow the procedure indicated in the previous example for the general setting.

Suppose that on \mathbf{R} we are given two multiresolution analyses, say $\dots \subset V_{-1}^i \subset V_0^i \subset V_1^i \subset \dots$ with scaling functions $\phi_i(x)$ and corresponding wavelets $\psi_i(x)$ where $i = 1, 2$. The subspaces $F_j \subset L_2(\mathbf{R}^2)$ are defined [Woj] as

$$F_j = V_j^1 \otimes V_j^2.$$

The sequence of subspaces $(F_j)_{j \in \mathbf{Z}}$ has the following properties:

$$\dots \subset F_{-1} \subset F_0 \subset F_1 \subset \dots \tag{7.1}$$

$$\overline{\bigcup_{j \in \mathbb{Z}} F_j} = L^2(\mathbb{R}^2) \quad (7.2)$$

$$\bigcap_{j \in \mathbb{Z}} F_j = \{0\} \quad (7.3)$$

$$f(x, y) \in F_j \Leftrightarrow f(2x, 2y) \in F_{j+1} \quad (7.4)$$

$$f(x, y) \in F_0 \Leftrightarrow f(x-1, y-1) \in F_0 \quad (7.5)$$

The system $\{\phi_1(x-k)\phi_2(y-l)\}_{(k,l) \in \mathbb{Z}^2}$

is an orthonormal basis in F_0 . (7.6)

If we write $V_1^i = V_0^i \oplus W_0^i$ for $i = 1, 2$ then we infer that

$$\begin{aligned} F_1 &= V_1^1 \otimes V_1^2 = (V_0^1 \oplus W_0^1) \otimes (V_0^2 \oplus W_0^2) \\ &= (V_0^1 \otimes V_0^2) \oplus (V_0^1 \otimes W_0^2) \oplus (W_0^1 \otimes V_0^2) \oplus (W_0^1 \otimes W_0^2) \\ &= F_0 \oplus (V_0^1 \otimes W_0^2) \oplus (W_0^1 \otimes V_0^2) \oplus (W_0^1 \otimes W_0^2). \end{aligned}$$

We also infer that

$\{\psi_1(x-k)\psi_2(y-l)\}_{k,l \in \mathbb{Z}}$ is an orthonormal basis in $W_0^1 \otimes W_0^2$

$\{\psi_1(x-k)\phi_2(y-l)\}_{k,l \in \mathbb{Z}}$ is an orthonormal basis in $W_0^1 \otimes V_0^2$

$\{\phi_1(x-k)\psi_2(y-l)\}_{k,l \in \mathbb{Z}}$ is an orthonormal basis in $V_0^1 \otimes W_0^2$

Using (7.1)-(7.6) we get three functions $\tilde{\psi}_1 = \psi_1 \otimes \psi_2$, $\tilde{\psi}_2 = \psi_1 \otimes \phi_2$ and $\tilde{\psi}_3 = \phi_1 \otimes \psi_2$ such that the system $\{\tilde{\psi}_i(2^j x - k, 2^j y - l)\}$ with $j, k, l \in \mathbb{Z}$ and $i = 1, 2, 3$ is an orthonormal basis in $L_2(\mathbb{R}^2)$.

Chapter 8

Compression on the Unit Sphere

One of the most common applications of wavelet theory is data compression. There are two kinds of compression schemes: lossless and lossy. In the case of lossless compression one is interested in reconstructing the data exactly, without any loss of information. We consider here lossy compression. This means we are ready to accept an error, as long as the quality after compression is acceptable. With lossy compression schemes we potentially can achieve much higher compression ratios than with lossless compression.

8.1 Image compression

Let us take the case of digitized images. The compression ratio is defined as the number of bits the initial image takes to store on the computer divided by the number of bits required to store the compressed image. This is easy to understand when we consider the fact that to store a moderately large image, say a 512×512 pixels, 24 bit color image, takes about 0.75 MBytes. This is only for still images; in the case of video, the situation becomes even worse. Then, we need this kind of storage for each frame, and we have something like 30 frames per second. This is just one reason why compression is important.

First, let us define, somewhat mathematically, what we mean by an image.

Let us for simplicity discuss an $L \times L$ gray scale image with $256 = 2^8$ gray scales (i.e., 8 bit). This can be considered to be a piecewise constant function defined on a square

$$f(x, y) = p_{ij} \in \mathbf{N}, \text{ for } i \leq x < i+1 \text{ and } j \leq y < j+1 \text{ and } 0 \leq i, j < L,$$

where $0 \leq p_{ij} \leq 255$. Let us fix an orthogonal wavelet ψ . Given an integer $M \geq 1$, we try to find the "best" approximation of f by using a representation

$$f_M(x, y) = \sum_{jk} c_{jk} \psi_{jk}(x, y)$$

with M nonzero coefficients c_{jk} .

The basic reason why this potentially might be useful is that each wavelet picks up information about the image f essentially at a given location and at a given scale. Where the image has many interesting features, we can expand many coefficients, and where the image is smooth we can use fewer coefficients and still achieve a high quality approximation. In other words, the wavelet transform allows us to focus on the most relevant parts of f . Now, to give this a mathematical meaning we need to agree on an error measure. Ideally, for image compression we should use a norm that corresponds as closely as possible to the human eye [D-J-L]. However, let us make it simple and discuss the case of L^2 .

So we are interested in finding an optimal approximation minimizing the error $\|f - f_M\|_{L^2}$. Because of the orthogonality of the wavelets,

$$\left(\sum_{jk} |(f, \psi_{jk}) - c_{jk}|^2\right)^{\frac{1}{2}}$$

is an equivalent measure. A moment's thought reveals that the best way to pick M nonzero coefficients c_{jk} , making the error as small as possible, is by simply picking the M coefficients with largest absolute value, and setting $c_{jk} = (f, \psi_{jk})$ for these numbers. This then yields the optimal approximation f_M^{opt} .

We can summarize wavelet image compression using the L^2 norm in three steps:

1. Compute coefficients c_1, \dots, c_m representing an image in a normalized two-dimensional wavelet basis.
2. Sort the coefficients in order of decreasing magnitude to produce the sequence $c_{\sigma(1)}, \dots, c_{\sigma(m)}$.
3. Starting with $\tilde{m} = m$, find the smallest \tilde{m} for which $\sum_{i=\tilde{m}+1}^m (c_{\sigma(i)})^2 \leq \epsilon^2$, where ϵ is the allowable L^2 error.

8.2 Pseudocode for compression

The pseudocode below outlines an efficient method that uses a binary search strategy to find a threshold below which coefficient sizes are deemed

negligible. The procedure takes as input a one-dimensional array of coefficients C (with each coefficient corresponding to a two-dimensional basis function) and an error tolerance ϵ . For each guess at a threshold τ , the algorithm computes the square of the L^2 error that would result from discarding coefficients smaller in magnitude than τ . This squared error s is compared to ϵ^2 at each iteration to decide whether the binary search should continue in the upper or lower half of the current interval. The algorithm halts when the current interval is so narrow that the number of coefficients to be discarded no longer changes.

procedure Compress (C: array [1..m] of reals; ϵ : real)

$\tau_{min} \leftarrow \min\{|C[i]|\}$

$\tau_{max} \leftarrow \max\{|C[i]|\}$

do

$\tau \leftarrow (\tau_{min} + \tau_{max})/2$

$s \leftarrow 0$

for $i \leftarrow 1$ **to** m **do**

if $|C[i]| < \tau$ **then** $s \leftarrow s + (C[i])^2$

end for

if $s < \epsilon^2$ **then** $\tau_{min} \leftarrow \tau$ **else** $\tau_{max} \leftarrow \tau$

until $\tau_{min} \approx \tau_{max}$

```

for  $i \leftarrow 1$  to  $m$  do
  if  $|C[i]| < \tau$  then  $C[i] \leftarrow 0$ 
end for
end procedure

```

However, DeVore *et al.* [D-J-L] suggest that the L^1 norm is best suited to the task of image compression.

8.3 An example of data compression on the unit sphere

The most well known spherical wavelets, namely by Freedon and Windheuser [F-W] and Schroder and Sweldens [S-S] assume regular gridpoints. In practice, the observed data are often irregularly distributed. Such scattered data are often encountered in global environmental studies, based on ground stations or on satellites [Le], [V-G-L]. To overcome this problem of irregularity, one can use the strictly positive definite functions studied in Chapter 2 to interpolate the scattered data in order to have regular data available.

In applications such as climatology, the earth is often regarded as a sphere of unit radius so that a meteorological variable $T(\boldsymbol{n})$, such as the sea level pressure or the surface air temperature, can be treated as spherical field. In this expression, $\boldsymbol{n} := [\cos \phi \cos \theta, \cos \phi \sin \theta, \sin \phi]^T$ denotes the unit vector

that points to a location on the earth from the center of the sphere, with ϕ and θ being the latitude and longitude of the location.

In many applications, the field $T(n)$ is observed only at a finite number of observing sites. If the observations denoted by $\{(T_j, n_j)\}_{j=1}^N$, are free of measurement error, then $T_j = T(n_j)$. A more realistic model is $T_j = T(n_j) + \epsilon_j$, where ϵ_j represents the additive noise. We will ignore the additive noise because it does not affect the presentation of the proposed methodology.

The data contains the monthly sea-level pressure (SLP) from January 1871 to December 1994 in millibars. The monthly grid resolution is 5 degrees \times 10 degrees (longitude, latitude). Therefore there are $72 \times 36 = 2592$ grid-points. The data are organized in full 360 degree latitude circles beginning at 90S and stepping northward to 90N. Along each circle (there are 36 circles) there are 72 points, the first value on a latitude line is matched to 0E longitude, and the last value is 355E (or equivalently 5W) longitude.

Let us briefly review some basic facts about the SLP. The pressure measured at each weather station is adjusted to the corresponding temperature at sea level in order to monitor properly horizontal changes in pressure. For any site above sea level, this adjustment is performed by assuming that a column of air, with a particular temperature profile, exists between the elevation of the station and sea level. Using this temperature profile, the conversion

to sea level pressure is calculated by increasing the station pressure by 10 millibars for every 100 m of elevation. Therefore, the approximate equation to reduce the measured pressure at a station to sea level is

$$P(\text{sea level}) = P(\text{observed}) + \frac{10\text{mb}}{100\text{m}} \cdot h$$

where h is the height above sea level.

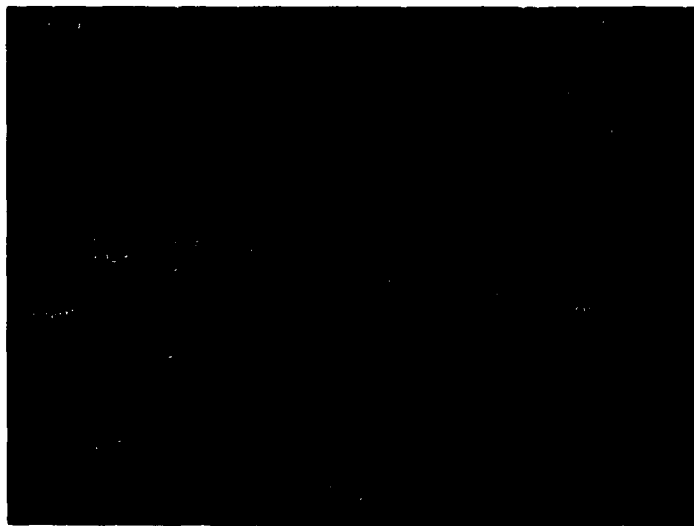


FIGURE 7. Sea-level pressure across the United States

The chart in figure 7 is useful for finding regions of high and low pressure systems. The solid contours represent pressure contours (isobars) in millibars. The isobars have an interval of 4 millibars. The wind speed is directly related to the distance between the isobars. The closer they are

together, the stronger the pressure gradient, and the stronger the wind. Low and high pressure systems can also be located from the map above. Low pressure systems are located in the regions of the lowest pressure, while high pressure systems are located in the regions of highest pressure. A high pressure center is where the pressure has been measured to be the highest relative to its surroundings. That means, moving in any direction away from the "High" will result in a decrease in pressure. A high pressure center also represents the center of an anticyclone and is indicated on a weather map by an "H".

A low pressure center is where the pressure has been measured to be the lowest relative to its surroundings. That means, moving in any horizontal direction away from the "Low" will result in an increase in pressure. Low pressure centers also represent the centers of cyclones. A low pressure center is indicated on a weather map by an "L" and winds flow counterclockwise around a low in the northern hemisphere. The opposite is true in the southern hemisphere, where winds flow clockwise around an area of low pressure. January 1986 and August 1986 will be the two cases used in the analysis.

After this brief introduction of SLP, our attention will be on compressing the available SLP data. A compactly supported biorthogonal spline wavelet "Bior3.9" is used in this analysis. After compressing our data, we show the

surfaces and contours of the original and approximated data; we have plotted also the surface of the details.

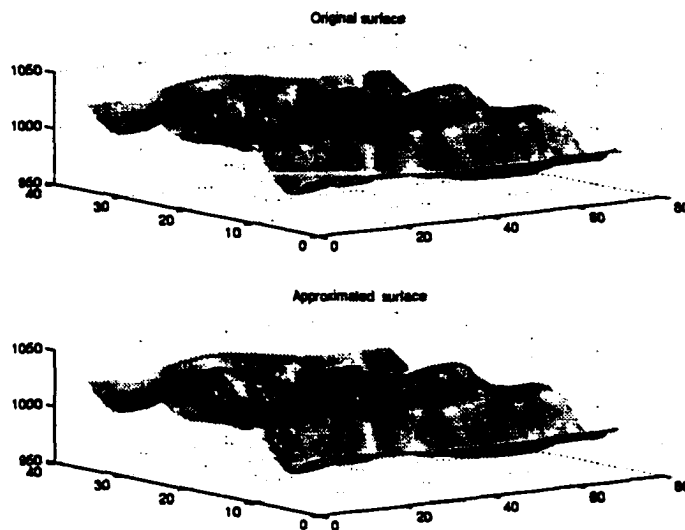


FIGURE 8. SLP surface plots for January 1986

For the case of January 1986, 69% of the wavelet coefficients are set to zero, and the percentage of the original signal's energy preserved is 100%. For the case of August 1986, the percentage of the wavelet coefficients that are set to zero is 70%, and the percentage of the original signal's energy preserved is 100%. Note that, even though the compressed signal is reconstructed using only 30% of the original signal, there is almost no detectable deterioration in the image quality of the two surfaces or the contour plots. The detail projection surfaces are very low compared to the original surfaces.

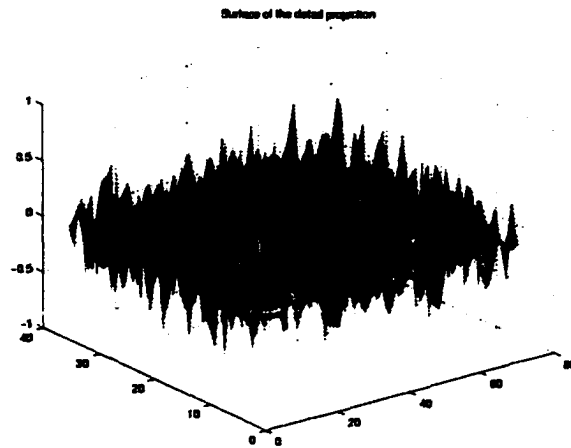


FIGURE 9. SLP detail surface for January 1986

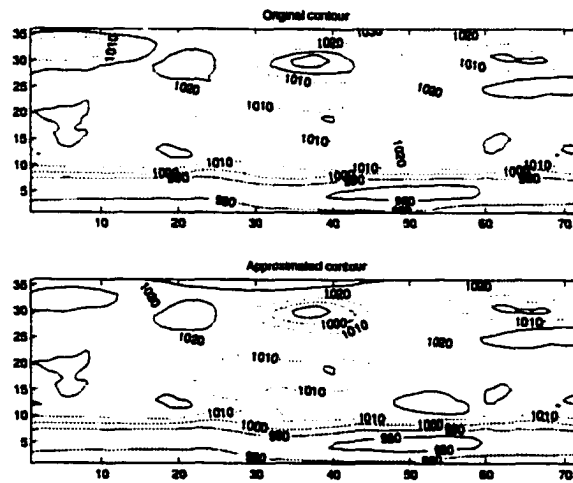


FIGURE 10. SLP contour plots for January 1986

As one can see from the figures and percentages, the previous analysis

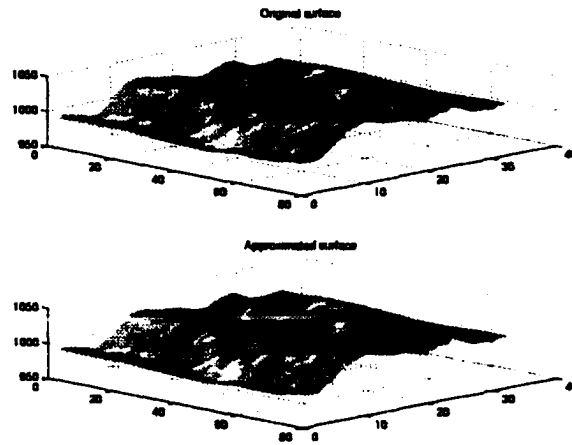


FIGURE 11. SLP surface plots for August 1986

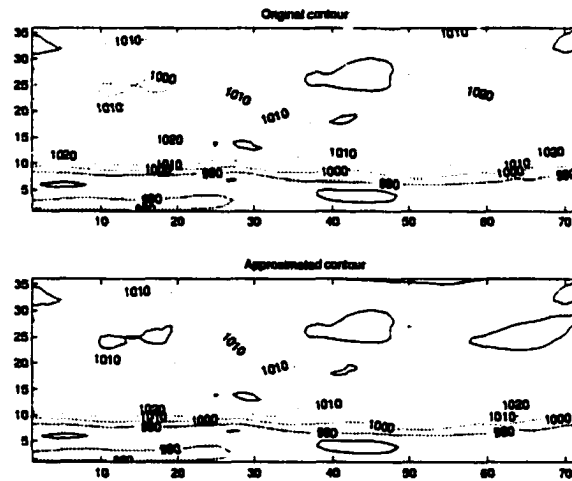


FIGURE 12. SLP contour plots for August 1986

gives satisfactory results, however this approach is practical only when the

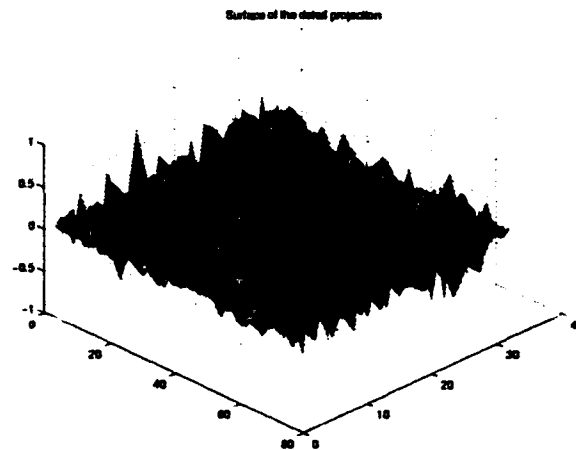


FIGURE 13. SLP detail surface for August 1986

data are grided and no concentrations around the poles are observed. In the next section we discuss this issue.

8.4 A general method for spherical compression

Let us briefly review recent constructions of wavelets on manifolds with special emphasis on the sphere.

The approach of Schröder and Sweldens [S-S] is based on a quasi-uniform icosahedral triangulation of the sphere. It allows a fast wavelet transform with computational cost growing linearly in the number of grid points. Numerical experiments show very good results for applications concerning the compression and fitting of data. Nevertheless, the scaling functions in their

approach cannot be evaluated exactly unless at the grid points, and it is not clear whether their construction yields a stable L^2 -basis.

Jaffard and Meyer [J-M] construct orthonormal wavelet bases on very general class of domains in \mathbb{R}^n . This idea applies as well to manifolds, but it uses an explicit orthonormalization procedure which requires Gram matrices to be inverted. The wavelets have good global support but do not allow for a fast wavelet transform.

To our knowledge, up to now the only discrete construction that exploits the topological structure of the sphere, in particular its rotational invariance, and requires neither a fixed coordinate system nor triangulation, has been undertaken by Freeden and his co-workers (see [F-S] and the references therein). They construct radially symmetric wavelets with arbitrary smoothness. A fast wavelet transform is described in [Sc]; the extension to closed surfaces is given in [F-S]. Dahlke *et al.* [D-D-S-W] follow a tensor product approach using exponential splines. Their construction is based on a fixed chart for the sphere. It yields C^1 -wavelets, but suffers from some problems at the poles when projecting functions onto the wavelet spaces, and the computer implementation seems to be difficult. This approach is extended to stable biorthogonal spherical wavelets in Weinreich's Ph.D. thesis [Wei]. In a similar spirit, Potts *et al.* [P-S-T] use tensor products of trigonometric

and algebraic polynomials to construct interpolatory spherical wavelets with global support that allow a fast wavelet transform. Again the poles are exceptional points since the underlying grid accumulates there. Hence, as in [D-D-S-W], these wavelets are not able to detect singularities at the poles.

Dahmen and Schneider [D-S] developed a very powerful, but abstract method for the construction of wavelet bases on smooth manifolds. The concept of stability and efficiency of multiscale transforms is discussed there in great detail, but their construction of wavelets relies on some prerequisites that are hard to realize for general manifolds. The theoretical background for their work can be found in [Da]; also in [C-D-P] some applications are given.

In addition to the discrete constructions, there are some papers on continuous wavelet transforms on the sphere. Dahlke and Maaß [D-M] construct wavelets on tangent bundles of spheres. Torresani [To] exploits the Weyl-Heisenberg group representation. Finally, Holschneider's approach [Ho] is based on dilations and rotations using stereographic projections.

We propose a method for compressing functions on the sphere based solely on a Ramanujan set of rotations and planar wavelets. This method was inspired by the fact that a rigorous method needs to perform uniformly well independently of the location of the support of the function on the

sphere, and for functions supported in a small (relatively flat) subset of S^2 , this method should be similar to the one obtained from the theory of wavelets on \mathbb{R}^2 , which is described in chapter 7.

The 2-sphere S^2 can not be embedded homeomorphically into the Euclidean plane \mathbb{R}^2 . For, if a topological mapping of S^2 onto a subset M of \mathbb{R}^2 existed, then M would be, like S^2 , compact and simply connected and consequently isomorphic to the closed disk. The Euler number of the disk ($\chi = 1$), however, differs from that of the sphere ($\chi = 2$). Thus there is no atlas of S^2 which consists of only one chart. To put it another way, every chart of the sphere has a singularity. This fact, known to cartographers for many centuries, complicates the positioning of points on the sphere considerably.

Let

$$SP : S^2 \setminus \{\text{North Pole}\} \rightarrow \mathbb{R}^2$$

be the stereographic projection, (see [Mü]). Let Ψ be an orthonormal basis of $L^2(\mathbb{R}^2)$ constructed using tensor products of some orthogonal wavelet basis of $L^2(\mathbb{R})$, (see Chapter 7). Let $SP^*(\Psi) \subseteq L^2(S^2)$ be the orthonormal basis of $L^2(S^2)$ obtained by pulling back the functions from Ψ to the sphere, and normalizing them appropriately, using the Jacobian of the stereographic projection. Then $SP^*(\Psi)$ is an orthonormal basis of $L^2(S^2)$. However, the members of this basis supported near the South Pole look very different

than the members supported near the North Pole as the North Pole is a singular point. In order to avoid this singularity we shall rotate the North Pole, using a well distributed set of rotations, namely a Ramanujan set of rotations discussed in Chapter 3 of this thesis. What follows is a description of our new method for compressing functions on the unit sphere.

Let $F(\xi_1, \xi_2, \xi_3)$ be a function belonging to $L^2(S^2)$. We project it onto the complex plane via the stereographic projection SP . Let us find first the Jacobian J of this transformation, taking into consideration the fact that $\xi_1^2 + \xi_2^2 + \xi_3^2 = 1$

$$J = \frac{1}{\begin{vmatrix} \frac{\partial x}{\partial \xi_1} & \frac{\partial x}{\partial \xi_2} \\ \frac{\partial y}{\partial \xi_1} & \frac{\partial y}{\partial \xi_2} \end{vmatrix}}.$$

Furthermore, we have

$$\frac{\partial \xi_3}{\partial \xi_1} = \frac{-\xi_1}{\xi_3} \quad \text{and} \quad \frac{\partial \xi_3}{\partial \xi_2} = \frac{-\xi_2}{\xi_3}.$$

Using this fact we have the following expression for J

$$J = \frac{1}{\begin{vmatrix} \frac{1-\xi_3-\xi_1^2}{(1-\xi_3)^2} & \frac{-\xi_1\xi_2}{\xi_3} \\ \frac{-\xi_1\xi_2}{\xi_3} & \frac{1-\xi_3-\xi_2^2}{(1-\xi_3)^2} \end{vmatrix}}.$$

After simplification we get

$$J = \frac{-1}{\xi_3(1-\xi_3)^2}.$$

The previous expression can be written in terms of $z = \frac{\xi_1 + i\xi_2}{1 - \xi_3}$. If we write ξ_3 in terms of z as

$$\xi_3 = \frac{|z|^2 - 1}{1 + |z|^2}$$

then an expression of $|J|$ in terms of z is

$$|J(z)| = \frac{4|1 - |z|^2|}{1 + |z|^2}.$$

The new function on the complex plane is

$$f(x, y) = F\left(\frac{2x}{1 + |z|^2}, \frac{2y}{1 + |z|^2}, \frac{|z|^2 - 1}{1 + |z|^2}\right) \cdot |J(z)|^{\frac{1}{2}}$$

where $z = x + iy$ and $|z| = \sqrt{x^2 + y^2}$.

Using the two dimensional wavelets on the plane we can therefore expand f in terms of the wavelet basis in $L^2(\mathbb{R}^2)$. For any function $f \in L^2(\mathbb{R}^2)$ we have

$$f(x, y) = \sum_{i=1}^3 \sum_{j,k,l} (f, \tilde{\psi}_i(2^j x - k, 2^j y - l)) \tilde{\psi}_i(2^j x - k, 2^j y - l)$$

where $\tilde{\psi}_1 = \psi_1 \otimes \psi_2$, $\tilde{\psi}_2 = \psi_1 \otimes \phi_2$ and $\tilde{\psi}_3 = \phi_1 \otimes \psi_2$ with $j, k, l \in \mathbb{Z}$. Refer to Chapter 7 for the definition of ψ_1 , ϕ_2 , ϕ_1 and ϕ_2 .

Decomposing the function we get

$$f(x, y) = A_{\gamma_0}(x, y) + D_{\gamma_0}(x, y)$$

where A_{γ_0} , and D_{γ_0} are respectively the approximation function and the detail function on the plane. As no rotation is performed, we have used

$\gamma_0 = id$. The next step in the algorithm is to rotate the function F on the unit sphere and then project it to the complex plane, but as the rotation group $SO(3)$ is mapped onto $SU(2)$, with homographic action on \mathbb{C} :

$$z \mapsto \frac{az + b}{cz + d}, \quad \begin{pmatrix} a & b \\ c & d \end{pmatrix} \in SU(2)$$

we will project F first onto the plane and then use the above transformation which is much easier to implement than the regular 3×3 rotations on the sphere. The scheme goes as follow:

$$F(\xi_1, \xi_2, \xi_3) \longrightarrow f(z) \longrightarrow f\left(\frac{az + b}{cz + d}\right) \cdot \frac{1}{|cz + d|^2}$$

where $z = \frac{\xi_1 + i\xi_2}{1 - \xi_3}$. Furthermore, the matrix $\begin{pmatrix} a & b \\ c & d \end{pmatrix}$ belongs to $\in SU(2)$ and it corresponds to reduced words formed by A_p , B_p , and C_p discussed in 4.1.

We decompose this new rotated function into the wavelet basis functions to get this time the approximation and detail functions A_{γ_j} and D_{γ_j} where γ_j belongs to the Ramanujan set S_5^M . We choose the set S_5^M and not any other arbitrary set of rotations for the main reason that this set generates a uniform distribution on the sphere. Moreover we derived a precise formula in Proposition 5.5 that provides us with the number of spherical caps of radius h needed to cover the whole unit sphere. We have then

$$f(\Re(\bar{z}), \Im(\bar{z})) = A_{\gamma_j}(\Re(\bar{z}), \Im(\bar{z})) + D_{\gamma_j}(\Re(\bar{z}), \Im(\bar{z}))$$

where

$$\bar{z} = \frac{a_j z + b_j}{c_j z + d_j},$$

and

$$\begin{pmatrix} a_j & b_j \\ c_j & d_j \end{pmatrix} \in SU(2).$$

Suppose that we stop this process at level M , then we need to pick the rotation that will assure the best approximation, say γ_{j_0} . We may choose γ_{j_0} so that

$$\|A_{\gamma_{j_0}}(\Re(\bar{z}), \Im(\bar{z}))\| = \max_{\gamma_j \in S_8^M} \|A_{\gamma_j}(\Re(\bar{z}), \Im(\bar{z}))\|.$$

Using the following decomposition

$$f(\Re(\bar{z}), \Im(\bar{z})) = A_{\gamma_{j_0}}(\Re(\bar{z}), \Im(\bar{z})) + D_{\gamma_{j_0}}(\Re(\bar{z}), \Im(\bar{z})),$$

the details and approximations at the first level of resolution are at hand, we can compress now the function on the plane based on the procedure of 8.2 to get $\tilde{f}(\Re(\bar{z}), \Im(\bar{z}))$ as the compressed function.

The original $F(\xi_1, \xi_2, \xi_3)$ is defined on the unit sphere, hence the compressed function needs to be projected and rotated back on the sphere. This time, the rotation will precede the projection because we are still processing signals on the complex plane. If

$$\bar{z} = \frac{az + b}{cz + d}$$

then

$$z = \frac{-d\bar{z} + b}{c\bar{z} - a}.$$

The rotation $\gamma_{j_0}^{-1}$ is associated with $\begin{pmatrix} \bar{a}_{j_0} & \bar{b}_{j_0} \\ \bar{c}_{j_0} & \bar{d}_{j_0} \end{pmatrix}$ which satisfy

$$\begin{pmatrix} \bar{a}_{j_0} & \bar{b}_{j_0} \\ \bar{c}_{j_0} & \bar{d}_{j_0} \end{pmatrix} = \begin{pmatrix} -d_{j_0} & b_{j_0} \\ c_{j_0} & -a_{j_0} \end{pmatrix}$$

where $\begin{pmatrix} a_{j_0} & b_{j_0} \\ c_{j_0} & d_{j_0} \end{pmatrix}$ is the matrix associated with γ_{j_0} . Note that both matrices $\begin{pmatrix} a_{j_0} & b_{j_0} \\ c_{j_0} & d_{j_0} \end{pmatrix}$ and $\begin{pmatrix} \bar{a}_{j_0} & \bar{b}_{j_0} \\ \bar{c}_{j_0} & \bar{d}_{j_0} \end{pmatrix}$ belong to $SU(2)$.

The function \tilde{f} is now a function of $\Re(z)$ and $\Im(z)$ where $z = \frac{-d\bar{z} + b}{c\bar{z} - a}$.

The final step in the algorithm is to use the inverse stereographic projection to pull back the function \tilde{f} to the unit sphere. The Jacobian of the inverse stereographic projection is

$$\frac{1}{J} = -\xi_3(1 - \xi_3)^2.$$

Finally, the compressed function \tilde{F} on the unit sphere is

$$\tilde{F}(\xi_1, \xi_2, \xi_3) = \tilde{f}\left(\frac{2\Re(z)}{1 + \|z\|^2}, \frac{2\Im(z)}{1 + \|z\|^2}, \frac{|z|^2 - 1}{1 + |z|^2}\right) \cdot \frac{1}{|J(z)|^{\frac{1}{2}}}.$$

For the algorithm to perform uniformly well independently of the location of the support of the function on the sphere we shall show that functions supported on a small region Ω of S^2 benefit from the proposed algorithm. This will follow from the next theorem.

Theorem 8.4.1. *The algorithm described above is based on a finite set of numbers (finite impulse response filters). Suppose a function $f \in L^2(S^2)$ is supported in a spherical cap Ω_h , of radius h centered at $\xi \in S^2$. Let Ω denote the spherical cap of radius $2h$ centered at the south pole $(0,0,-1)^T$. Let $M > 0$ be the smallest integer satisfying the following inequality:*

$$\frac{\log n}{\sqrt{n}} < \frac{\sqrt{5}(\log 5)\pi^2}{12\sqrt{2}(\sqrt{5}+1)(16+\sqrt{\pi})} h^{\frac{3}{2}}, \text{ where } n = \frac{3}{2}(5^M - 1).$$

Then there is a rotation $\gamma_0 \in S_5^M$ such that $\gamma_0\Omega_h \subseteq \Omega$. In particular, our algorithm will approximate the function f as well as if f was supported in Ω . As a consequence, the performance of the algorithm does not depend on the location of the support of the function f .

Proof. The main components of our algorithm are the three matrices A_p , B_p , and C_p described in 4.1, and the wavelet finite impulse response filters on the plane. Therefore, the algorithm is based on a finite set of numbers.

We have shown in Proposition 5.5 that if M is the level of rotations of S_5^M , then it suffices that n satisfies the following inequality for the covering of the unit sphere to be achieved

$$\frac{\log n}{\sqrt{n}} < \frac{\sqrt{5}(\log 5)\pi^2}{12\sqrt{2}(\sqrt{5}+1)(16+\sqrt{\pi})} h^{\frac{3}{2}}, \text{ where } n = \frac{3}{2}(5^M - 1).$$

So

$$\bigcup_{\gamma \in S_5^M} \gamma\Omega_h = S^2.$$

Hence

$$\Omega \subseteq \bigcup_{\gamma \in S_5^M} \gamma \Omega_h.$$

Since the radius of Ω is twice larger as the radius of Ω_h we see that there is a $\gamma_0 \in S_5^M$ such that

$$\gamma_0 \Omega_h \subseteq \Omega.$$

Therefore, the performance of the algorithm is checked for any arbitrary region on the unit sphere. \square

Chapter 9

Concluding Remarks

This dissertation presents contributions to research in the field of mathematics and digital signal processing on the sphere. The main goal is two fold: (i) Study interpolation, equidistribution and covering on the sphere using mathematical tools such as the representation theory. (ii) Develop an algorithm using planar wavelets and the Ramanujan set of rotations S_5^M to compress functions on the unit sphere.

We give first definitions of positive definite functions in the case of the real line and in the case of the m -sphere. Then after defining strictly positive definite functions, we give a sufficient condition for a zonal function to be a strictly positive definite. A major result of this thesis is that we have proven Shreiner's result as a consequence of a more general representation-theoretic result, namely for compact groups using tools from the Representation Theory.

The other major direction of this thesis is to compress square integrable functions on the unit sphere. The main tools used in this analysis are a Ramanujan set of rotations and planar wavelets. Ramanujan sets of rotations are introduced and our focus is on S_5^M , a special set from the Ramanujan set of rotations. Starting with a point on the digital sphere lying on none of the

coordinate axes and using S_5^M points on the sphere are generated. Examples showing the performance of the uniformity of the equidistribution of these generated points is studied in terms of quadrature on the sphere.

An important application to time-frequency representations is presented. The proposed method is to detect abrupt spectral changes in noisy signals. The performance of the proposed method is shown in different experiments. The results clearly justify the new approach. A precise formula to cover the unit sphere with a given radius is derived. Furthermore, using this formula, an algorithm to compress functions on the unit sphere is developed.

For further research, completely characterizing functions which are strictly positive definite on the sphere needs to be investigated. Furthermore, an optimal formula for covering the sphere should be targeted. Moreover, the algorithm needs to be implemented for practical problems. Addressing these types of questions using the available algorithm will possibly generate insight and help compress signals on the unit sphere efficiently.

REFERENCES

- [A-P] Allali, M. & Przebinda, T., *Strictly Positive Definite Functions on a Compact Group*, To appear in Proceedings of the AMS.
- [C] Cui, J., *Finite Pointset Methods on the Sphere and their Application in Physical Geodesy*, Ph.D. thesis, University of Kaiserslautern, Geomathematics Group, Germany.
- [C-D-P] Carnicer, J. and Dahmen, W. & Peña, J., *Local Decomposition of Refinable Spaces and Wavelets*, Appl. Comput. Harm. Anal. **3** (1996), 127-153.
- [C-M-Q-W] Coifman, R., Meyer, Y., Quake, S., & Wickerhauser, M., *Signal Processing and Compression With Wave Packets*, Proceedings of the International Conference on Wavelets (1989), Y. Meyer, ed., Masson, Paris.
- [D] Dieudonné, D., *Eléments d'Analyse*, Gauthier-Villars Editeur, Paris/Bru-xelles/Montréal, 1975.
- [Da] Daubechies, I., *Orthonormal Bases of Compactly Supported Wavelets*, Comm. Pure Appl. Math. **41** (1988), 909-996.
- [Do] Donoho, D., *De-noising by Soft-thresholding*, IEEE Trans. Inform. Theory **41** (1995), 613-627.
- [D-D-S-W] Dahlke, W., Dahmen, W., Schmitt, E. & Weinreich, I., *Multiresolution Analysis and Wavelets on S^2 and S^3* , Numer. Funct. Anal. Optimiz. **16** (1995), 19-41.
- [D-J-L] DeVore, A., Jawerth, B. & Lucier, B., *Surface Compression*, Comput. Aided Geom. Des. **9** (1992), 219-239.
- [D-M] Dahlke, S. & Maab, P., *Continuous Wavelet Transform with Applications to Analyzing Functions on Spheres*, Fourier Anal. Appl. **2** (1995), 379-396.
- [D-Mi] Dyn, N. & Micchelli, C., *Interpolation by Sums of Radial Functions*, Numer. Math. **58** (1990), 1-9.
- [D-S] Dahmen, W. & Schneider, R., *Composite Wavelet Bases for Operator Equations*, report 133, IGPM, RWTH, Aachen (1996).
- [F] Franklin, P., *A Set of Continuous Orthogonal Functions*, Math. Ann. **100** (1928), 522-529.
- [Fl] Flandrin, P., *Some Aspects of Nonstationary Signal Processing with Emphasis on Time-frequency and Time-scale*, Wavelets, Time-frequency Methods and Phase Space, Berlin: Springer, IPTI, 68-98.
- [Fr] Franke, R., *Scattered Data Interpolation: Tests of Some Methods*, Math. Comp. **38** (1982), 181-200.
- [F-S] Fasshauer, G. & Schumaker, L., *Data Fitting on the Sphere*, Mathematical Methods

- for Curves and Surfaces II (1998), 117-166.
- [Fr-S] Freedon, W. & Schreiner, M., *Orthogonal and Non-orthogonal multiresolution Analysis, Scale Discrete and Fully Discrete Wavelet Transform on the Sphere*, AGTM-Report 163, AG Geomathematik, University of Kaiserslautern (1996).
- [F-V-R] Flandrin, P., Vidalie, B. & Rioul, O., *Fourier and Wavelet Spectrograms Seen as Smoothed Wigner-ville Distributions*, Proc. Int. Conf. Wavelets and Applications, Marseille, France (1989), 95.
- [F-W] Freedon, W. & Windheuser, U., *Combined Spherical Harmonic and Wavelet Expansion - A Future Concept in Earth's Gravitational Determination*, Appl. Comput. Harm. 4 (1997), 1-37.
- [Gu] Gutzmer, T., *Interpolation by Positive Definite Functions on Locally Compact Groups with Applications to $SO(3)$* , Results in Mathematics 29 (1996), 69-77.
- [H] Haar, A., *Zur Theorie der Orthogonalen Funktionen-systeme*, Math. Ann. 69 (1910), 331-371.
- [H-R] Hewitt, E. & Ross, K., *Abstract Harmonic Analysis, Volume II*, Springer-Verlag, New York, 1970.
- [Ho] Holschneider, M., *Continuous Wavelet Transforms on the Sphere*, Math. Phys. 37 (1996), 4156-4165.
- [J-M] Jaffard, S. & Meyer, Y., *Bases d'Ondelettes dans des Ouverts de \mathbb{R}^n* , Math. Pures Appl. 68 (1989), 95-108.
- [K] Kirillov, A., *Elements of the Theory of Representations*, Springer-Verlag, New York, 1976.
- [K-B] Kadambe, S. & Boudreaux-Bartels, G., *Application of the Wavelet Transform for Pitch Detection of Speech Signals*, IEEE Trans. Inform. Theory 38 (March 1992), 917-924.
- [Le] Leroy, S., *Measurements of Geopotential Heights by GPS Radio Occultation*, Geophysical Research 102 (1997), 6971-6986.
- [L-D] Laurent, H. & Doncarli, C., *Stationarity Index for Abrupt Changes Detection in the Time-frequency Plane*, IEEE Signal Processing Lett. 5, no.2 (February 1998), 43-45.
- [L-H] Li, T. & Hinich, M., *A Filter Bank Approach for Modeling and Forecasting Seasonal Patterns*, Tech. Report 355, Department of statistics and Applied Probability, University of California, Santa Barbara (1998).
- [L-M] LeMarié, P. & Meyer, Y., *Ondelettes et Bases Hilbertiennes*, Rev. Mat. iberoamericana 2 (1986), 1-18.
- [L-P-S] Lubotzky, A., Phillips, R. & Sarnak, P., *Hecke Operators and Distributing Points on the Sphere I*, Comm. Pure Appl. Math. 39 (1986), 149-186.
- [M] Mallat, S., *Multiresolution Approximation and Wavelet Orthonormal Bases of $L^2(\mathbb{R})$* , Trans. Amer. Math. Soc. 315 (1989), 69-87.

- [Mi] Micchelli, C., *Interpolation of Scattered Data: Distances, Matrices, and Conditionally Positive Definite Functions*, *Constr. Approx.* **2** (1986), 11-22.
- [Mü] Müller, C., *Analysis of Spherical Symmetries in Euclidean Spaces*, Springer-Verlag, 1998.
- [M-H] Mallat, S. & Hwang, W., *Singularity Detection and Processing with Wavelets*, *IEEE Trans. Inform. Theory* **38** (March 1992), 917-924.
- [N-W] Narcowich, F. & Ward, J., *Norm Estimates for the Inverses of a General Class of Scattered-data Radial-function Interpolation Matrices*, *Approx. Theory* **69** (1992), 84-109.
- [P-S-T] Potts, D., Steidel, G. & Tashe, M., *Kernels of Spherical Harmonics and Spherical Frames*, World Scientific (1996), 1-154.
- [R] Rudin, W., *Real and Complex Analysis*, McGraw-Hill, New York, 1974.
- [S] Schreiner, M., *On a New Condition For Strictly Positive Definite Functions On Spheres*, *Proceedings of the AMS* **125** (1997), 531-539.
- [Sa] Sasvári, Z., *Positive Definite and Definitizable Functions*, Akademic-Verlag, Berlin, 1994.
- [Sc] Schoenberg, I., *Positive Definite Functions On Spheres*, *Duke Math. J.* **9** (1942), 96-108.
- [Sl] Sloane, N., *Encrypting by Random Rotations*, *Cryptograph, Lecture Notes in computer Science* **149** (1983), Springer-Verlag, Berlin, 522-529.
- [St] Strömberg, J., *A Modified Franklin System and Higher Order Spline Systems on \mathbb{R}^n as Unconditional Bases for Hardy Spaces*, in *Conference on Harmonic Analysis in Honor of Antoni Zygmund*, B. et al., ed., II (1928), Univ. of Chicago Press, Chicago.
- [Sz] Szegő, G., *Orthogonal Polynomials*, AMS, Coll. Publ. XXIII, 1939.
- [S-S] Schröder, P. & Sweldens, W., *Spherical Wavelets: Efficiently Representing Functions on the Sphere*, *Computer Graphics Proceedings ACM Siggraph* (1995), 161-165.
- [S-W] Shaback, R. & Wu, Z., *Operators on Radial Functions*, *Comput. Appl. Math.* **73** (1996), 1-17.
- [T] Tichy, R., *Random Points in the Cube and on the Sphere with Applications to Numerical Analysis*, *Comput. Appl. Math.* **31** (1990), 191-197.
- [To] Torresani, B., *Local Fourier Analysis on Spheres*, Preprint (1993).
- [V-G-L] Vinnikov, K., Groisman, P. & Lugina, K., *Empirical Data on Contemporary Global Climate Changes (Temperature and Precipitation)*, *Climate* **3** (1990), 662-677.
- [We] Wendland, H., *Piecewise Polynomial, Positive Definite and Compactly Supported Radial Functions of Minimal Degree*, *Adv. Comp. Math.* **4** (1995), 389-396.
- [Wei] Weinreich, I., *Biorthogonale Wavelets auf der Sphäre*, Dissertation, Shaker Verlag (1997).

[Wu] Wu, Z., *Multivariate Compactly Supported Positive Definite Radial Functions*, *Adv. Comp. Math.* 4 (1995), 283-292.

[X-C] Xu, Y. & Cheney, E., *Strictly Positive Definite Functions on Spheres*, *Proceedings of the AMS* 118 (1992), 977-981.

APPENDIX A
CODE FOR GENERATING POINTS ON THE UNIT SPHERE

```

function x=lps(n)

% This program generates points on the unit sphere
% using  $S_5^M$ . It uses the matrices  $A_p$ ,  $B_p$  and  $C_p$ 
% defined in section 4.1.

n=input('How many levels?')

% Produces matrices  $A_p$ ,  $B_p$  and  $C_p$  and their inverses.

R(:,1)=(1/sqrt(5))*[1+2i 0;0 1-2i];
R(:,2)=(1/sqrt(5))*[1 2;-2 1];
R(:,3)=(1/sqrt(5))*[1 2i;2i 1];
R(:,4)=inv(R(:,1));
R(:,5)=inv(R(:,2));
R(:,6)=inv(R(:,3));

% Starting point
x(1)=(1+i)/(sqrt(3)-1);

% Generates points up to level n
for m=1:(6^n - 1)/5.0
    for j=1:6
        if mod(m-1,6)==0
            k=6;
        else
            k=rem(m-1,6);
        end
    end
end

```

```

if abs(k-j)==3
    x(6*m-5+j)=0;
else
    a=R(1,1,j)*x(m)+R(1,2,j);
    b=R(2,1,j)*x(m)+R(2,2,j);
    x(6*m-5+j)=a/b;
    Mag=1+(abs(x(6*m-5+j)))2;
    a=(2*real(x(6*m-5+j)))/Mag;
    b=(2*imag(x(6*m-5+j)))/Mag;
    c=(Mag-2)/Mag;
    y(:,6*m-5+j)=[a,b,c];
end
end
end

```

APPENDIX B
CODE FOR FREQUENCY-HOPPED SIGNALS

```
function si=hopp(p)

%This program measures the stationarity index of discrete data.

% The signal is frequency-hopped signal at t = 180, 210 and 240.

% SS = output

% t = time

% f = frequency

% create a set of data with abrupt changes–frequency hopping

l=0:1000;

k=linspace(0,pi,512);

y1=sin(.2*k*1000);

y2=sin(.3*k*1000);

y3=sin(.25*k*1000);

s1=[y1(1,1:179) zeros(1,(512-179))];

s2=[zeros(1,179) y2(1,180:209) zeros(1,(512-209))];

s3=[zeros(1,209) y3(1,210:239) zeros(1,(512-239))];

s4=[zeros(1,239) y1(1,240:512)];

ss=s1+s2+s3+s4;

% We introduce here Gaussian noise.

wn=randn(size(512)); %white noise

ss1=ss/norm(ss);

wn1=wn/norm(wn);

Pss=ss1+ss1';
```

```

Pwn=wnl*wnl';

SNR=10*log10(Pss/Pwn),disp('dB')

% The signal is corrupted with noise

SS=ss1+wnl;

% Plot the spectrogram of the signal

subplot(2,2,1),specgram(SS,512,1000,boxcar(15),12)

title('Spectrogram');

xlabel('Time')

ylabel('Frequency')

% Calculates Kolmogorov distance

[B,F,T]=specgram(SS,512,1000,boxcar(15),12);

m=size(F)

n=size(T)

disp('Wait.....')

Bn=B/norm(B);

disp('Wait.....')

if p==1

    for i=2:n

        d1(:,1)=abs(abs(Bn(:,i))-abs(Bn(:,i-1)));

        si(i,1)=sum(d1,1);

    end

    size(si)

else

    for i=p:n-p

```

```

    for k=1:p
        d1(:,1)=abs(abs(Bn(:,i+k))-abs(Bn(:,(i-p+k)))));
        d11sum(k,1)=sum(d1,1);
    end
    si(i,1)=sum(d11sum,1);
end
size(d11sum);
[u,v]=size(si);
end
subplot(2,2,2),plot(T(25:(u-5)),si(25:(u-5),1))
axis tight
title('Original Method')
xlabel('Time')
ylabel('Index of Stationarity')
% Continuous wavelet analysis
% Uses "Daubechies-4"
M=cwt(SS,1:6,'db4');
% perform Kolmogorov on wavelet coefficient d1
[b,f,t]=specgram(M(2,:),512,1000,boxcar(15),12);
m1=size(f);
n1=size(t);
disp('In the process of calculation. Wait.....')
bn=b/norm(b); %normalize each row
if p==1

```

```

for i=2:n1

    d1(:,1)=abs(abs(bn(:,i))-abs(bn(:,i-1)));

    si(i,1)=sum(d1,1);

end

size(si);

else

    for i=p:n1-p

        for k=1:p

            d1(:,1)=abs(abs(bn(:,i+k))-abs(bn(:,(i-p+k)))));

            d11sum(k,1)=sum(d1,1);

        end

        si(i,1)=sum(d11sum,1);

    end

    size(d11sum);

    [u,v]=size(si);

end

subplot(2,2,3),plot(t(25:(u-5)),si(25:(u-5),1))

axis tight

title('Hybrid Method')

xlabel('Time')

ylabel('Index of Stationarity')

b=cwt(SS,1:1,'db4');

[m1,n1]=size(b);

disp('In the process of calculation. Wait.....')

```

```

bn=b/norm(b); %normalize each row

if p==1

    for i=2:n1

        d1(:,1)=abs(abs(bn(:,i))-abs(bn(:,i-1)));

        si(i,1)=sum(d1,1);

    end

    size(si);

else

    for i=p:n1-p

        for k=1:p

            d1(:,1)=abs(abs(bn(:,i+k))-abs(bn(:,(i-p+k)))));

            d11sum(k,1)=sum(d1,1);

        end

        si(i,1)=sum(d11sum,1);

    end

    size(d11sum);

    [u,v]=size(si);

end

subplot(2,2,4),plot((20:(u-5)),si(20:(u-5),1))

axis tight

title('Direct Method')

xlabel('Time')

ylabel('Index of Stationarity')

axis tight

```



```
disp('press enter to continue')
```

```
pause
```

```
end
```

APPENDIX C
CODE FOR CHIRP SIGNALS

```
function h=chirp1(p)

% This program measures the stationarity index of discrete data.

% The signal is a chirp with abrupt changes at t = 180, 210 and 240.

% SO = output

% t = time

% f = frequency

% creates a set of data with abrupt changes-chirp

t=0:0.001:4;

y1=chirp(t,100,1,200,'q');

y2=chirp(t,200,1,300,'q');

y3=chirp(t,250,1,400,'q');

s1=[y1(1,3001:3179) zeros(1,(512-179))];

s2=[zeros(1,179) y2(1,3001:3030) zeros(1,(512-209))];

s3=[zeros(1,209) y3(1,3001:3030) zeros(1,(512-239))];

s4=[zeros(1,239) y1(1,3240:(3240+511-239))];

ss=s1+s2+s3+s4;

% to vary the SNR of the data

for i=1:2

wn=randn(size(512));

ss1=i*ss/norm(ss);

wn1=wn/norm(wn);

Pss=ss1+ss1';
```

```

Pwn=wn1*wn1';
SNR=10*log10(Pss/Pwn),disp('dB')
% The signal is corrupted with noise
SO=ss1+wn1;
% calculates the Kolmogorov distance [B,F,T]=specgram(SO,512,1000,boxcar(15),12);
m=size(F)
n=size(T)
disp('Wait.....')
Bn=B/norm(B); %normalize each row
disp('Wait.....')
if p==1
    for i=2:n
        d1(:,1)=abs(abs(Bn(:,i))-abs(Bn(:,i-1))));
        si(i,1)=sum(d1,1);
    end
    size(si)
else
    for i=p:n-p
        for k=1:p
            d1(:,1)=abs(abs(Bn(:,i+k))-abs(Bn(:,i-p+k))));
            d11sum(k,1)=sum(d1,1);
        end
        si(i,1)=sum(d11sum,1);
    end
end

```

```

size(d11sum);

[u,v]=size(si);

end

subplot(2,2,2),plot(t(25:(u-5)),si(25:(u-5),1))

axis tight

title('Original Method')

xlabel('Time')

ylabel('Index of Stationarity')

% Uses "daubechies-4"

M=cwt(SO,1:6,'db4');

subplot(2,2,1),spectrogram(M(1,:),512,1000,boxcar(15),12);

title('Spectrogram')

xlabel('Time')

ylabel('Frequency')

% perform Kolmogorov on wavelet coefficient d1

[b,f,t]=spectrogram(M(1,:),512,1000,boxcar(15),12);

n1=size(T)

disp('In the process of calculation. Wait.....')

bn=b/norm(b); %normalize each row

if p==1

    for i=2:n1

        d1(:,1)=abs(abs(bn(:,i))-abs(bn(:,i-1)));

        si(i,1)=sum(d1,1);

    end

end

```

```

size(si);
else
for i=p:n1-p
for k=1:p
d1(:,1)=abs(abs(bn(:,i+k))-abs(bn(:,(i-p+k)))));
d11sum(k,1)=sum(d1,1);
end
si(i,1)=sum(d11sum,1);
end
size(d11sum);
[u,v]=size(si);
end
subplot(2,2,3),plot(t(25:(u-5)),si(25:(u-5),1))
axis tight
title('Hybrid Method')
xlabel('Time')
ylabel('Index of Stationarity')
[b,f,t]=specgram(M(2,:),512,1000,boxcar(15),12);
bn=b/norm(b); %normalize each row
if p==1
for i=2:n1
d1(:,1)=abs(abs(bn(:,i))-abs(bn(:,i-1)));
si(i,1)=sum(d1,1);
end

```

```

size(si);
else
    for i=p:n1-p
        for k=1:p
            d1(:,1)=abs(abs(bn(:,i+k))-abs(bn(:,(i-p+k))));
            d11sum(k,1)=sum(d1,1);
        end
        si(i,1)=sum(d11sum,1);
    end
    size(d11sum);
    [u,v]=size(si);
end
subplot(2,2,4),plot(t(25:(u-5)),si(25:(u-5),1))
axis tight
title('Direct Method')
xlabel('Time')
ylabel('Index of Stationarity')
disp('press enter to continue')
pause
end

```